JM PAPERS

Water wave propagation through arrays of closely spaced surface-piercing vertical barriers

J. Huang[1],† and R. Porter[1]

[1]School of Mathematics, University of Bristol, Woodland Road, Bristol BS8 1UG, UK

This paper presents and compares two different approaches to solving the problem of wave propagation across a large finite periodic array of surface-piercing vertical barriers. Both approaches are formulated in terms of a pair of integral equations, one exact and based on a spacing $\delta > 0$ between adjacent barriers and the other approximate and based on a continuum model formally developed by using homogenisation methods for small δ. It is shown that the approximate method is simpler to evaluate than the exact method which requires eigenvalues and eigenmodes related to propagation in an equivalent infinite periodic array of barriers. In both methods, the numerical effort required to solve problems is independent of the size of the array. The comparison between the two methods allows us to draw important conclusions about the validity of homogenisation models of plate array metamaterial devices. The practical interest in this problem stems from the result that for an array of barriers there exists a critical value of radian frequency, ω_c, dependent on δ, below which waves propagate through the array and above which it results in wave decay. When $\delta \to 0$, the critical frequency is given by $\omega_c = \sqrt{g/d}$, where d is the plate submergence and g is the acceleration due to gravity, which relates to the resonance in narrow channels and is an example of local resonance, studied extensively in metamaterials. The results have implications for proposed schemes to harness energy from ocean waves and other problems related to rainbow trapping and rainbow reflection.

Key words: wave scattering

1. Introduction

Problems involving the reflection and transmission of waves by thin vertical surface-piercing barriers under classical linearised theory have been the subject of research

† Email address for correspondence: jin.huang@bristol.ac.uk

over many decades. For a fluid of infinite depth, Ursell (1947) obtained an explicit solution for monochromatic waves normally incident upon a single barrier. When the fluid has a constant finite depth, Porter & Evans (1995) showed how to obtain accurate numerical solutions which provide upper and lower bounds on reflected and transmitted amplitudes by formulating complementary integral equations. They also produced numerical results for a pair of identical surface-piercing barriers, reproducing and extending results of Evans & Morris (1972), Newman (1974) and McIver (1985). Notably, Newman (1974) had shown, using matched asymptotic methods, that a pair of closely spaced barriers can totally transmit or reflect incoming wave energy at angular frequencies in the vicinity of a critical value of $\omega_c = \sqrt{g/d}$ related to the vertical fluid resonance in the narrow column between the two vertical plates, where d is the depth of submergence of the plates and g is the acceleration due to gravity. Evans (1978) later used this idea to model the operation of a narrow oscillating water column wave energy device. Non-identical barriers and arrays of more than two barriers have been considered by a number of authors including Evans & Porter (1997) and Roy, De & Mandal (2019).

More recently, Wilks, Montiel & Wakes (2022) have considered larger arrays of closely spaced barriers whose submergence increases gradually in the direction of the incident wave, i.e. so-called 'graded array'. The graded array is a specific type of metamaterial that refers to a material designed to have specific properties not found in naturally occurring materials and typically consists of repeating sub-wavelength structures. The graded array in Wilks *et al.* (2022) is designed to be resonant at multiple frequencies associated with the variable fluid column lengths across the array such that high reflection is sustained across a broad range of frequencies, known as rainbow reflection. Similar ideas based on local internal resonance provided by the displacement of the surface have been implemented in water waves using C-ring cylinders in channels, rather than vertical barriers, by Dupont *et al.* (2017), Bennetts, Peter & Craster (2018), Archer *et al.* (2020), etc. Large arrays of floating buoys which resonate on the surface of the fluid with elements that either possess constant properties or vary in space have been considered for wave energy harvesting applications by, for example, Garnaud & Mei (2009) and Porter (2021), as well as by Wilks *et al.* (2022). Arrays of resonators have been used to produce similar rainbow reflection on acoustic wave transmission in waveguides in the form of cavities attached to sidewalls (e.g. Tang 2012; Jiménez *et al.* 2017; Jan & Porter 2018) and on surface wave propagation in elasticity (e.g. Colquitt *et al.* 2017) in the form of mechanical oscillators attached to the surface of an elastic half-space.

In this paper, we return to consider large periodic arrays of surface-piercing vertical barriers which are equally spaced and submerged to the same constant depth, being simpler than the graded array problem. Part of the motivation for looking at this problem is to characterise the effects of resonance on models which are based on low-frequency homogenisation of plate array structures. This approximation replaces the discrete structure of the array by a continuous effective medium under an assumed contrast in scales between the wavelength and the spacing between plates. This approximation allows problems of a large array of closely spaced plates to be solved more easily and has been used to consider the interaction of waves with metamaterial structures (e.g. Jan & Porter 2018; Liu *et al.* 2018; Zheng, Porter & Greaves 2020). Away from resonant conditions, results from homogenisation of plate array structures compare favourably with those derived from the application of direct numerical methods for discrete arrays (e.g. Zheng *et al.* (2020) and Porter, Zheng & Liang (2022), where comparison is made with boundary integral methods). However, low-frequency homogenisation fails when undamped fluid motion in narrow channels is resonant, occurring at the critical frequency

ω_c indicated above. This is an example of the well-known phenomenon of local resonance in metamaterials (e.g. Ma & Sheng 2016).

By assuming a periodic array with barriers having an equal depth of submergence, d, we allow ourselves the opportunity of making an analytic comparison between a direct solution of the discrete array of $N + 1$ plates separated by a non-zero distance δ and homogenisation methods based on $\delta/d \ll 1$ in order to understand issues relating to resonance. In particular, periodicity allows us to exploit Bloch–Floquet methods which are associated with the corresponding infinite periodic arrays. When considering the scattering by a finite number of identical elements arranged periodically in an array, a naive approach is to apply direct multiple scattering methods, which leads to a large coupled system (examples are given in Linton & McIver (2001)). For quasi-one-dimensional scattering systems, such as the one we consider here, transfer and scattering matrices are often used to reduce the computational effort, in which wave information is propagated left and right (see Porter & Porter 2003; Wilks *et al.* 2022). For the transfer matrix method, reflection and transmission across the array are expressed as products of matrices which encode the scattering characteristics of a single element by converting incoming modes consisting of both propagating and a truncated set of evanescent waves into outgoing modes. This becomes impractical when considering closely spaced arrays since the size of the matrix must increase to capture a greater number of mode interactions as the value of δ/d is decreased. Results showed that for an infinite periodic array there exist ranges of frequencies for which wave propagation through the structure is prohibited. For the constrained mass system in Wilks *et al.* (2022), they argued that they must replace scattering matrices in favour of a formulation involving a system of integral equations which link certain functions at the nth barrier to corresponding functions at the $(n \pm 1)$th barriers since the wave scattering problem and the equations of motion are needed to be solved simultaneously.

The frequency ranges indicated above for which wave propagation through the periodic structures is absolutely forbidden are well known as stop bands and the corresponding structure is called the band-gap structure. It is shown that the existence of stop bands is possible for one-dimensional periodically varying topography (e.g. Porter & Porter 2003; An & Ye 2004). Further, Chen *et al.* (2004) and Yang *et al.* (2006) investigated the band-gap structures of liquid surface waves propagating through an infinite two-dimensional periodic topography of circle and square hollows, respectively. McIver (2000) and Linton (2011) also established the existence of a band-gap structure associated with water waves propagating over infinite periodic arrays of submerged vertical and horizontal cylinders. If an incident wave is subjected to a finite section of this infinite array at a certain frequency within such a stop band, most of energy is expected to be reflected.

In this paper we take a new approach to determining the scattering by periodic arrays of finite extent and develop concepts introduced in the work of Porter & Porter (2003) who highlighted connections between finite- and infinite-array problems. Specifically, they showed that the transfer matrices referred to above could be expressed in terms of generalised eigenvalues and eigenfunctions of the corresponding periodic Bloch–Floquet problem representing both propagating and decaying modes. After specifying the infinite periodic array problem in §2 we introduce a novel orthogonality relation satisfied by the Bloch eigenfunctions, which is key to developing a solution in the interior of the array. Then we present two different forms of solution for the Bloch–Floquet problem by expanding the velocity potential with different orthogonal functions, each of which has its own advantages in numerical calculation. Information is now able to propagate

from the left to the right of the array of $N + 1$ barriers via a simple product of Bloch wavenumbers/eigenvalues; this is described in § 4 of the paper.

In § 3 we formally develop the homogenisation approximation for a continuum model, which relies on a separation of horizontal length scales based on the wavelength and the array separation, δ. It turns out this assumption is violated as the resonance of fluid in the narrow channels is approached since solutions are predicted with a propagating wavelength which tends to zero. The wave scattering problem of this continuum model is solved in § 5. Numerical results are produced to show the comparison between the exact description of the finite array and the approximation based on homogenisation in order to demonstrate how the Bloch–Floquet solution produces accurate and efficient results and to demonstrate when homogenisation is a reliable approach to take. The work is summarised in § 6.

It is worth pointing out that as the spacing between plates tends to zero, viscous effects become important in the physical setting. Since our primary interest is to understand the resonance occurring in metamaterial structures and to evaluate the validity of homogenisation, the effect of viscosity is not taken into account in the present paper. For a consideration of the viscous effects the reader is referred to Mei, Stiassnie & Yue (2005), whose idea has been implemented to consider the energy dissipation in the metamaterial (see Zheng *et al.* 2020).

2. The periodic barrier problem

Consider an infinite periodic array of thin barriers with equal spacing δ, which extend vertically downwards to a depth d below the free surface of a fluid with constant depth h. Two-dimensional Cartesian coordinates are defined with the origin O in the mean free surface and z directed vertically upwards, such that barriers occupy $\{x = x_n = n\delta$ $(n \in \mathbb{Z}), -d < z < 0\}$.

Under the assumption of an incompressible and inviscid fluid and irrotational flow, the fluid motion of a single frequency ω can be described by $\text{Re}\{\phi(x, z) \exp(-\mathrm{i}\omega t)\}$ (in which t is time), where the spatial velocity potential $\phi(x, z)$ satisfies

$$\nabla^2 \phi = 0, \quad \text{in the fluid.} \tag{2.1}$$

On the free surface, the combined linearised kinematic and dynamic boundary conditions result in

$$K\phi - \phi_z = 0, \quad \text{on } z = 0, \tag{2.2}$$

where $K = \omega^2/g$. No-flow conditions apply on fixed rigid boundaries meaning

$$\phi_x = 0, \quad \text{on } x = n\delta^{\pm} \quad (n \in \mathbb{Z}) \quad \text{for } -d < z < 0, \tag{2.3}$$

where the positive and negative signs denote two sides of the plate, and

$$\phi_z = 0, \quad \text{on } z = -h. \tag{2.4}$$

Besides, the analysis of the flow close to the edge of the barrier reveals that the fluid velocity should possess inverse square root behaviour. Finally, since the geometry is periodic we may invoke the Bloch–Floquet theory which allows us to consider just one periodic element of the array (here we choose $D = \{0 < x < \delta, -h < z < 0\}$) provided we introduce quasi-periodic boundary conditions on those fluid interfaces which connect one cell to the next. For our choice of D, we require

$$\left.\begin{array}{l} \phi(\delta, z) = \mathrm{e}^{\mathrm{i}\beta\delta}\phi(0, z) \\ \phi_x(\delta, z) = \mathrm{e}^{\mathrm{i}\beta\delta}\phi_x(0, z) \end{array}\right\} \quad \text{for } -h < z < -d, \tag{2.5}$$

where β is the Bloch wavenumber needed to be determined.

Momentarily it helps to imagine that λ replaces $\mathrm{e}^{\mathrm{i}\beta\delta}$ in (2.5). Since the problem is unchanged by the mapping $x \to \delta - x$, if λ is an eigenvalue then λ^{-1} is another eigenvalue. Also, if ϕ is a solution corresponding to λ then $\bar{\phi}$, the complex conjugate of ϕ, is also a solution with eigenvalue $\bar{\lambda}$. This implies that eigenvalues λ must lie either on the real axis in reciprocal pairs or on the unit circle in complex conjugate pairs. Returning to β, this implies that β is a real number or can be expressed as $n\pi/\delta + \mathrm{i}\gamma_n$ (where $n \in \mathbb{Z}$ and $\gamma \in \mathbb{R}$) and that for every β it is paired with $-\beta$.

When β is real, it represents a wavenumber which encodes the phase shift of the fluid motion as waves propagate across one cell of the infinite periodic array. We note that we need only consider real values of $\beta \in (0, \pi/\delta]$ since $\beta' = \beta + 2\pi m/\delta$ for $m \in \mathbb{Z}$ leaves the problem unchanged and $\beta' = 2\pi/\delta - \beta$ results in the same problem with x mapped to $\delta - x$. That is to say, it reverses the wave direction, but not the solution. When β becomes a complex number, for similar reasons we only need to consider the case of β being $n\pi/\delta + \mathrm{i}\gamma_n$ ($n = 0, 1$ and $\gamma_n \in \mathbb{R}^+$). These values represent a solution with local wave decay from one cell to the next (i.e. evanescent waves) although the extension to the infinite periodic array is unphysical.

It can be shown that there is only one real value of β which exists below one certain frequency and one complex value of $\beta = \pi/\delta + \mathrm{i}\gamma_1$ that exists above the certain frequency, which means they will not appear at the same frequency. Meanwhile, there exist a number of pure imaginary values of $\beta = \mathrm{i}\gamma_0^{(k)}$ ($k = 1, 2, \ldots$) over the whole frequency range. Thus, we can label different values of β as $\beta = \pm\beta^{(k)}$ ($k = 0, 1, 2, \ldots$), where $k = 0$ is reserved for an eigenvalue either on the positive real axis or in the complex plane and $k = 1, 2, \ldots$ are used for the pure imaginary values which are ordered with increasing magnitude along the imaginary axes.

The boundary-value problem described above is homogeneous (that is, free of forcing) and we can think of β as playing the part of the eigenvalue and $\phi \neq 0$ the corresponding eigenfunction. Thus, each eigenvalue $\pm\beta^{(k)}$ will be associated with a corresponding eigenfunction which is labelled as $\phi = \phi^{(\pm k)}(x, z)$ such that

$$\phi^{(-k)}(x, z) = \phi^{(+k)}(\delta - x, z), \tag{2.6}$$

resulting in $\phi^{(-0)}(x, z)$ being different from $\phi^{(+0)}(x, z)$. In particular, this implies that

$$\phi^{(-k)}(0, z) = \exp(\mathrm{i}\beta^{(k)}\delta)\phi^{(+k)}(0, z) \tag{2.7}$$

and

$$\phi_x^{(-k)}(0, z) = -\exp(\mathrm{i}\beta^{(k)}\delta)\phi_x^{(+k)}(0, z), \tag{2.8}$$

which will be used extensively later.

2.1. *An orthogonality relation*

Before we set about solving the eigenproblem, we introduce a useful orthogonality relation. Consider two eigenfunctions $\phi^{(+k)}(x, z)$ and $\phi^{(\pm j)}(x, z)$ satisfying all of the

conditions of the problem described above. Then from Green's identity we have

$$0 = \iint_D \left[\phi^{(+k)} \nabla^2 \phi^{(+j)} - \phi^{(+j)} \nabla^2 \phi^{(+k)} \right] dx\, dz$$

$$= \int_S \left[\phi^{(+k)} \frac{\partial \phi^{(+j)}}{\partial n} - \phi^{(+j)} \frac{\partial \phi^{(+k)}}{\partial n} \right] ds$$

$$= \left[\exp(i(\beta^{(k)} + \beta^{(j)})\delta) - 1 \right] \int_{-h}^{-d} \left[\phi^{(+k)} \frac{\partial \phi^{(+j)}}{\partial x} - \phi^{(+j)} \frac{\partial \phi^{(+k)}}{\partial x} \right]_{x=0} dz \qquad (2.9)$$

and

$$0 = \iint_D \left[\phi^{(+k)} \nabla^2 \phi^{(-j)} - \phi^{(-j)} \nabla^2 \phi^{(+k)} \right] dx\, dz$$

$$= \int_S \left[\phi^{(+k)} \frac{\partial \phi^{(-j)}}{\partial n} - \phi^{(-j)} \frac{\partial \phi^{(+k)}}{\partial n} \right] ds$$

$$= \left[\exp(i(\beta^{(k)} - \beta^{(j)})\delta) - 1 \right] \int_{-h}^{-d} \left[\phi^{(+k)} \frac{\partial \phi^{(-j)}}{\partial x} - \phi^{(-j)} \frac{\partial \phi^{(+k)}}{\partial x} \right]_{x=0} dz, \qquad (2.10)$$

after using the conditions on the boundary, S, of D having elemental arclength ds and outward normal derivative $\partial/\partial n$. The factor in front of the integral in (2.10) is zero if $\beta^{(k)} = \beta^{(j)}$, while the factor in front of the integral in (2.9) cannot be zero except for $\beta^{(k)} = \beta^{(j)} = \pi/\delta$, where $k = j = 0$. Assuming for now that the eigenvalues $\beta^{(k)}$ are distinct and $\beta^{(0)} \neq \pi/\delta$, it follows the following orthogonality relation:

$$\int_{-h}^{-d} \left[\phi^{(+k)}(0, z) \frac{\partial \phi^{(+j)}}{\partial x}(0, z) - \phi^{(+j)}(0, z) \frac{\partial \phi^{(+k)}}{\partial x}(0, z) \right] dz = 0, \qquad (2.11a)$$

$$\int_{-h}^{-d} \left[\phi^{(+k)}(0, z) \frac{\partial \phi^{(-j)}}{\partial x}(0, z) - \phi^{(-j)}(0, z) \frac{\partial \phi^{(+k)}}{\partial x}(0, z) \right] dz = E^{(+k)} \delta_{kj}, \qquad (2.11b)$$

where $E^{(+k)}$ is a scaling factor defined by

$$E^{(+k)} = \int_{-h}^{-d} \left[\phi^{(+k)}(0, z) \frac{\partial \phi^{(-k)}}{\partial x}(0, z) - \phi^{(-k)}(0, z) \frac{\partial \phi^{(+k)}}{\partial x}(0, z) \right] dz$$

$$= -2 \int_{-h}^{-d} \phi^{(-k)}(0, z) \frac{\partial \phi^{(+k)}}{\partial x}(0, z)\, dz = -E^{(-k)}, \qquad (2.12)$$

after using (2.7) and (2.8).

The special case $\beta^{(0)} = \pi/\delta$ relates to standing waves in the cell and (2.6) no longer defines an independent second function since $\phi^{(0)}(x, z) = \phi^{(+0)}(x, z) = \phi^{(-0)}(x, z)$. Instead, we define $\phi^{(0)}(x, z)$ satisfying (2.5) by imposing supplementary constraints:

$$\phi^{(0)}(0, z) = \phi^{(0)}(\delta, z) = 0 \qquad (2.13)$$

or

$$\phi_x^{(0)}(0, z) = \phi_x^{(0)}(\delta, z) = 0, \qquad (2.14)$$

for $-h < z < -d$. It follows that $\phi_x^{(0)}(\delta/2, z) = 0$ or $\phi^{(0)}(\delta/2, z) = 0$ and the solutions here relate to sloshing modes in closed rectangular domains of width δ either with or

960 A20-6

without a vertical baffle along the centreline. For the latter case, it can be deduced that it happens at $K = (n\pi/\delta)\tanh(n\pi h/\delta)$ for $n = 1, 2, \dots$ (see Mei *et al.* 2005). Sloshing modes of similar character, but of more complex geometry, were shown to emerge in Porter & Porter (2003). Besides, it should be noted that the orthogonality relation (2.11) no longer applies for $\beta^{(0)} = \pi/\delta$.

2.2. *Solution of two independent forms*

There are many different approaches one could adopt to develop solutions to the single-cell problem which partly depend upon how the fundamental cell is defined. Since our choice of the fundamental cell, D, is rectangular with conditions on the boundary of D it makes sense to use separation of variables. In the following, we describe two different forms of solution for the Bloch–Floquet problem given above.

In the first form, the cell is divided into two subdomains which are above and below the level $z = -d$, and the solution is expanded by eigenfunctions in x. In $-d < z < 0$, we write the general solution satisfying (2.1), (2.2) and (2.3) as

$$\phi(x, z) = a_{1,0}(1 + Kz) + \sum_{n=1}^{\infty} a_{1,n}\cos(n\pi x/\delta)\zeta_n(z), \tag{2.15}$$

where

$$\zeta_n(z) = \frac{\cosh(n\pi z/\delta) + (K\delta/n\pi)\sinh(n\pi z/\delta)}{\cosh(n\pi d/\delta)}, \quad n \geq 1 \tag{2.16}$$

and $a_{1,n}$ for $n = 0, 1, \dots$ are coefficients to be determined. In $-h < z < -d$, the general solution of (2.1) satisfying (2.4) and (2.5) is

$$\phi(x, z) = \sum_{n=-\infty}^{\infty} b_{1,n}\frac{\cosh\beta_n(h + z)}{\cosh\beta_n(h - d)}\exp(i\beta_n x), \tag{2.17}$$

where

$$\beta_n = \beta + 2n\pi/\delta \tag{2.18}$$

and $b_{1,n}$ for $n \in \mathbb{Z}$ are also undetermined coefficients.

The pressure and vertical component of velocity must coincide across the common fluid interface $z = -d$ for $0 < x < \delta$. We first define

$$w(x) = \phi_z(x, -d), \quad 0 < x < \delta, \tag{2.19}$$

which represents the vertical velocity across $z = -d$. From (2.15) and the orthogonality of the cosine functions over $0 < x < \delta$, continuity of velocity allows us to write

$$a_{1,n} = \begin{cases} \dfrac{1}{K\delta}\displaystyle\int_0^\delta w(x)\,\mathrm{d}x, & n = 0, \\[2mm] \dfrac{2}{n\pi[K\delta - n\pi\tanh(n\pi d/\delta)]}\displaystyle\int_0^\delta w(x)\cos(n\pi x/\delta)\,\mathrm{d}x, & n \geq 1. \end{cases} \tag{2.20}$$

Also, from (2.17) we have, using orthogonality of the functions $e^{i\beta_n x}$ over $0 < x < \delta$,

$$b_{1,n} = \frac{1}{\beta_n\delta\tanh\beta_n(h - d)}\int_0^\delta w(x)\exp(-i\beta_n x)\,\mathrm{d}x, \quad n \in \mathbb{Z}. \tag{2.21}$$

960 A20-7

We now match pressure at $z = -d$ and substitute (2.19) and (2.20) for $a_{1,n}$ and $b_{1,n}$ to give the scalar homogeneous integral equation

$$\int_0^\delta w(x')\mathcal{L}(x, x')\, dx' = 0, \quad 0 < x < \delta, \tag{2.22}$$

where

$$\mathcal{L}(x, x') = \frac{Kd - 1}{K\delta} + 2\sum_{n=1}^{\infty} D_n \cos(n\pi x/\delta)\cos(n\pi x'/\delta) + \sum_{n=-\infty}^{\infty} \frac{\exp(i\beta_n(x - x'))}{\beta_n\delta \tanh \beta_n(h - d)} \tag{2.23}$$

and

$$D_n = \left(\frac{1}{n\pi}\right)\frac{(K\delta/n\pi)\tanh(n\pi d/\delta) - 1}{(K\delta/n\pi) - \tanh(n\pi d/\delta)} \sim \frac{1}{n\pi}, \tag{2.24}$$

as $n \to \infty$ (or as $\delta/d \to 0$).

The second form is to use eigenfunctions in the depth coordinate to expand the solution which is a natural approach to solving water wave problems (Linton & McIver 2001). This leads to the solution being posed in terms of integral equations over finite intervals of $x = 0$: either for the unknown $\phi_x(0, z)$ between $-h < z < -d$ or for the unknown $\phi(\delta^-, z) - e^{i\beta\delta}\phi(0^+, z)$ between $-d < z < 0$. Given the relation derived in § 2.1, the first of these two options is particularly attractive. Thus, the velocity potential is first written as

$$\phi(x, z) = \sum_{n=0}^{\infty} \left(a_{2,n}\, e^{k_n x} + b_{2,n}\exp(-k_n x)\right)\psi_n(z). \tag{2.25}$$

Here k_n are the roots of the dispersion equation

$$\omega^2/g = -k_n \tan k_n h, \tag{2.26}$$

where k_n ($n \geq 1$) is real and positive while $k_0 = -ik$ and k is the real positive wavenumber, and

$$\psi_n(z) = N_n^{-1/2}\frac{\cos k_n(z + h)}{\cos k_n h}, \tag{2.27}$$

with

$$N_n = \frac{1}{2\cos^2 k_n h}\left(1 + \frac{\sin 2k_n h}{2k_n h}\right), \tag{2.28}$$

which satisfy the orthogonality relation

$$\frac{1}{h}\int_{-h}^{0}\psi_n(z)\psi_m(z)\, dz = \delta_{mn}. \tag{2.29}$$

We now define

$$u(z) = \phi_x(0, z), \quad -h < z < -d, \tag{2.30}$$

which represents the horizontal velocity across $x = 0$. From the velocity periodic condition in (2.5) and the orthogonality relation in (2.29), we have

$$a_{2,n} = \frac{e^{i\beta\delta} - \exp(-k_n\delta)}{2k_n h \sinh k_n\delta}\int_{-h}^{-d} u(z)\psi_n(z)\, dz \tag{2.31}$$

and

$$b_{2,n} = \frac{e^{i\beta\delta} - e^{k_n\delta}}{2k_n h \sinh k_n\delta} \int_{-h}^{-d} u(z)\psi_n(z)\,dz. \tag{2.32}$$

Applying the pressure periodic condition in (2.5) with (2.31) and (2.32) results in another scalar homogeneous integral equation:

$$\int_{-h}^{-d} u(z')\mathcal{K}(z, z')\,dz' = 0, \quad -h < z < -d, \tag{2.33}$$

where

$$\mathcal{K}(z, z') = \sum_{n=0}^{\infty} \frac{\cos\beta\delta - \cosh k_n\delta}{k_n h \sinh k_n\delta} \psi_n(z)\psi_n(z'). \tag{2.34}$$

2.3. *Numerical approximation*

The numerical approximation of the integral equations is based on methods described in Porter & Evans (1995) in which it is recognised that the end points, $(0, -d)$ and $(\delta, -d)$, of the intervals involved in the integral equations coincide with the sharp edges of the barriers and the fluid velocity behaves as the inverse square root of distance to the edge. Thus, for the first form given in the previous section we choose

$$w(x) \approx \sum_{m=0}^{M_1} \alpha_{1,m} w_m(x), \tag{2.35}$$

where

$$w_m(x) = \frac{T_m(2x/\delta - 1)}{\pi\sqrt{(\delta/2)^2 - (x - \delta/2)^2}}, \tag{2.36}$$

in which $T_m(\cdot)$ is a Chebyshev polynomial and M_1 is the designated truncation parameter. In what follows we use the results that follow from, for example, Erdélyi *et al.* (1954):

$$\int_0^\delta w_m(x)\cos(n\pi x/\delta)\,dx = \cos[(m+n)\pi/2]J_m(n\pi/2) \tag{2.37}$$

and

$$\int_0^\delta w_m(x)\exp(-i\beta_n x)\,dx = \exp(-i\beta_n\delta/2)\exp(-im\pi/2)J_m(\beta_n\delta/2), \tag{2.38}$$

where $J_m(\cdot)$ are the mth-order Bessel functions of the first kind. Substituting the approximation (2.35) into (2.22), multiplying through by $w_n(x)$ and integrating over

$0 < x < \delta$ result in the following system of equations for the expansion coefficients $\alpha_{1,n}$:

$$\sum_{n=0}^{M_1} \alpha_{1,n} L_{mn} = 0, \quad m = 0, 1, \ldots, M_1, \tag{2.39}$$

where

$$L_{mn} = \frac{Kd - 1}{K\delta} \delta_{m0}\delta_{n0} + 2 \sum_{r=1}^{\infty} D_r \cos\left[\frac{1}{2}(m+r)\pi\right]$$

$$\times \cos\left[\frac{1}{2}(n+r)\pi\right] J_m\left(\frac{1}{2}r\pi\right) J_n\left(\frac{1}{2}r\pi\right)$$

$$+ \exp(-i(m-n)\pi/2) \sum_{r=-\infty}^{\infty} \frac{J_m\left(\frac{1}{2}\beta_r\delta\right) J_n\left(\frac{1}{2}\beta_r\delta\right)}{\beta_r\delta \tanh \beta_r(h-d)}. \tag{2.40}$$

Similarly, for the second form we expand the unknown horizontal velocity $u(z)$ as

$$u(z) \approx \sum_{m=0}^{M_2} \alpha_{2,m} u_m(z) \tag{2.41}$$

in a series of $M_2 + 1$ prescribed functions:

$$u_m(z) = \frac{2(-1)^m T_{2m}[(h+z)/(h-d)]}{\pi\sqrt{(h-d)^2 - (h+z)^2}}, \tag{2.42}$$

which satisfy the condition (2.4) on the sea bed. Substituting the approximation (2.41) into (2.33), multiplying through by $u_n(z)$ and integrating over $-h < z < -d$ lead to the following system of equations for the expansion coefficients $\alpha_{2,n}$:

$$\sum_{n=0}^{M_2} \alpha_{2,n} K_{mn} = 0, \quad m = 0, 1, \ldots, M_2, \tag{2.43}$$

where

$$K_{mn} = \sum_{r=0}^{\infty} \frac{(\cos \beta\delta - \cosh k_r\delta)}{k_r h \sinh k_r\delta} F_{mr} F_{nr}, \tag{2.44}$$

in which we have defined

$$F_{mr} = \int_{-h}^{-d} u_m(z)\psi_r(z)\,dz = N_r^{-1/2} J_{2m}[k_r(h-d)]. \tag{2.45}$$

Numerically we fix Kd and look for real values of $\beta \in (0, \pi/\delta]$, $\gamma_1 > 0$ with $\beta = \pi/\delta + i\gamma$ and $\gamma_0^{(k)} > 0$ with $\beta = i\gamma_0^{(k)}$ for which the system of (2.39) or (2.43) has non-trivial solutions. When β is real the matrix formed by L_{mn} is Hermitian and when β is complex the matrix is real, while the matrix formed by K_{mn} is a real matrix no matter whether β is real or complex. These result in that the determinants of the two matrices are always real, so zero eigenvalue of the corresponding matrix can be found numerically using standard root-finding methods. In particular, when β becomes a pure imaginary number, from the

last term in (2.40) we can see that when $\gamma_0(h - d)$ passes across $k\pi$ each element in L_{mn} will tend to positive or negative infinity. Thus, it can be deduced that the overall behaviour of L_{mn} is similar to that of the function $\cot \gamma_0(h - d)$ and $\gamma_0^{(k)}(h - d) \in ((k - 1)\pi, k\pi)$ though the same conclusion is not easily drawn from K_{mn}. Furthermore, all of the series in L_{mn} and K_{mn} are convergent as of $O(1/r^2)$. In order to accelerate the numerical computation, an effective treatment is performed for these series (see Appendix A for details).

As is shown later, either of the two methods of solution presented above can be used to find accurate values of eigenvalues, β. However, accurately determining the eigenfunctions $\phi(x, z)$ is more problematic. Even though both methods use functions which accurately capture the inverse square root singularity at the lower edges of the barriers as part of the solution method, the expressions for ϕ are formed by separation solutions which do not explicitly include these singularities. Consequently, the expansion coefficients associated with the separation solutions are slowly convergent for both methods (like $O(1/n^{3/2})$). In order to produce plots of the eigenfunctions so that they may be compared with the results of homogenisation (in § 3.1) we nevertheless find that the first method works well. This is because when δ/d is small, which is the primary interest of the present study, only one or two terms are required in the expansion of the unknown velocity across the level $z = -d$ to obtain very accurate solutions whilst these separation solutions are well suited to close spacing with the first term in the expansion above and below $z = -d$ being dominant. This is not true, however, for the second method since evanescent modes play an important role when δ/d is small. Thus it is hard to plot eigenfunctions across the whole domain accurately by using the second method for small δ/d.

Also later, when we consider scattering by finite arrays using a discrete barrier method we are required to compute integrals over the intervals $-h < z < -d$ beneath the barriers involving the eigenfunctions and their derivative with respect to x. Although separation solutions for determining ϕ from the first method can do this accurately, the series in which derivatives are taken term-by-term are no longer convergent, with terms decreasing like $O(1/n^{1/2})$. For this reason, the second method is useful since the solution method provides highly accurate representations for the derivative which explicitly include the singularity at $z = -d$ as shown in (2.30) and (2.41).

2.4. *Small δ/d and $\beta\delta$*

We now assume that $\epsilon = \delta/d \ll 1$ and $\beta\delta \ll 1$, that is to say, $\beta d \ll 1/\epsilon$. Based on the solution in the first form presented in the previous section, the dominant entry in (2.40) is

$$L_{00} \approx \frac{Kd - 1}{K\delta} + \frac{1}{\beta\delta \tanh \beta(h - d)}, \tag{2.46}$$

after using $J_m(\beta\delta/2) \approx \delta_{m0}$ and assuming that $K\delta/|Kd - 1|$ has the same order as $\beta\delta$, i.e. $K\delta/|Kd - 1| \ll 1$. Thus, the leading-order approximation to values of β for small δ/d is determined from solving $L_{00} = 0$, or

$$\beta \tanh \beta(h - d) = \frac{K}{1 - Kd}, \tag{2.47}$$

provided $|1 - Kd|/Kd \gg \epsilon$ which implies that $|1 - Kd| \gg \epsilon$. As for the velocity potential, if we normalise α_n by setting $\alpha_0 = K\delta/(1 - Kd)$, after using (2.47) the velocity potential

can be written as

$$\phi(x, z) \approx \begin{cases} (1 + Kz)/(1 - Kd), & -d < z < 0, \\ e^{i\beta x} \cosh \beta(h + z)/\cosh \beta(h - d), & -h < z < -d. \end{cases} \tag{2.48}$$

From (2.48), we can see that when $\delta/d \ll 1$ and $\beta\delta \ll 1$, the expressions only including the first term ($n = 0$) in (2.15) and (2.17) are good at simulating the flat oscillation in the cell. Besides, (2.47) is similar to the dispersion equation (2.26) with $n = 0$. It can be proved that here β only can be real or pure imaginary but could not be a complex number and the real value exists only when $Kd < 1$.

3. A continuum model

In this section, we develop an approximation to wave propagation through the infinite periodic array by directly applying asymptotic methods to the underlying boundary-value problem. The principal assumption is that $\epsilon = \delta/d \ll 1$ (close spacing between adjacent barriers), which is the same as in § 2.4. In $-d < z < 0$, we make a multiple scales approximation, i.e. $x \to d\hat{x} + \delta X$, where $\hat{x}$ is the macroscale variable and X operates on the scale of a single cell. We also scale $z \to d\hat{z}$ and write

$$\phi(x, z) \approx \phi^{(0)}(\hat{x}, X, \hat{z}) + \epsilon\phi^{(1)}(\hat{x}, X, \hat{z}) + \epsilon^2\phi^{(2)}(\hat{x}, X, \hat{z}) + \cdots. \tag{3.1}$$

In $0 < X < 1$ and $-1 < \hat{z} < 0$, from (2.1) we have

$$\left[\frac{\partial^2}{\partial X^2} + 2\epsilon \frac{\partial}{\partial \hat{x} \partial X} + \epsilon^2 \left(\frac{\partial^2}{\partial \hat{x}^2} + \frac{\partial^2}{\partial \hat{z}^2} \right) \right] \left(\phi^{(0)} + \epsilon\phi^{(1)} + \epsilon^2\phi^{(2)} + \cdots \right) = 0, \tag{3.2}$$

with

$$\left(\frac{\partial}{\partial X} + \epsilon \frac{\partial}{\partial \hat{x}} \right) \left(\phi^{(0)} + \epsilon\phi^{(1)} + \epsilon^2\phi^{(2)} + \cdots \right) = 0, \quad \text{on } X = 0, 1 \tag{3.3}$$

and

$$\left(\frac{\partial}{\partial \hat{z}} - Kd \right) \left(\phi^{(0)} + \epsilon\phi^{(1)} + \epsilon^2\phi^{(2)} + \cdots \right) = 0, \quad \text{on } \hat{z} = 0. \tag{3.4}$$

Using (3.2) with (3.3) for the zero order gives

$$\phi^{(0)}(\hat{x}, X, \hat{z}) \equiv \phi^{(0)}(\hat{x}, \hat{z}), \tag{3.5}$$

which is independent of X. At the first order, (3.2) is

$$\frac{\partial^2\phi^{(1)}}{\partial X^2} = -2\frac{\partial^2\phi^{(0)}}{\partial \hat{x} \partial X} = 0, \tag{3.6}$$

where (3.5) has been applied. Integrating (3.6) over $0 < X < 1$ and using the boundary conditions implied by (3.3) for $\phi^{(1)}$ on $X = 0, 1$ give

$$\phi^{(1)} = -\frac{\partial\phi^{(0)}}{\partial \hat{x}}X + f(\hat{x}, \hat{z}), \tag{3.7}$$

where $f(\hat{x}, \hat{z})$ is a function independent of microscale variable X. Further, if we consider the second-order term in (3.2) and (3.3), we can obtain

$$\frac{\partial^2}{\partial X^2}\phi^{(2)} + 2\frac{\partial^2}{\partial \hat{x} \partial X}\phi^{(1)} + \left(\frac{\partial^2}{\partial \hat{x}^2} + \frac{\partial^2}{\partial \hat{z}^2} \right) \phi^{(0)} = 0, \tag{3.8}$$

with

$$\frac{\partial \phi^{(2)}}{\partial X} + \frac{\partial \phi^{(1)}}{\partial \hat{x}} = 0, \quad \text{on } X = 0, 1. \tag{3.9}$$

Again, integrating (3.8) over $0 < X < 1$ and applying (3.5), (3.7) and (3.9) result in

$$\frac{\partial^2 \phi^{(0)}}{\partial \hat{z}^2} = 0 \tag{3.10}$$

as the leading-order governing equation, with (3.4) applying at zeroth order. The general solution, satisfying (3.10), is $\phi^{(0)} = X(\hat{x})(1 + Kd\hat{z})$ for an arbitrary function $X(\hat{x})$. Since we are concerned with wave propagation, we write

$$\phi^{(0)}(\hat{x}, \hat{z}) = A \exp(i\mu d\hat{x})(1 + Kd\hat{z}), \tag{3.11}$$

where μ is a coefficient to be determined and the assumption is that $\mu d \ll 1/\epsilon$ otherwise the horizontal variation is not on the macroscale.

In $-h < z < -d$, since the fluid is not bounded by barriers, we can drop the microscale, resulting in that we rescale with $x \to d\hat{x}$ and $z \to d\hat{z}$. After expanding the velocity potential with respect to ϵ, we can find that $\phi^{(0)}(\hat{x}, \hat{z})$ still satisfies Laplace's equation:

$$\left(\frac{\partial^2}{\partial \hat{x}^2} + \frac{\partial^2}{\partial \hat{z}^2} \right) \phi^{(0)} = 0. \tag{3.12}$$

After applying the separation of variables, the solution of (3.12) satisfying the zeroth-order condition on the sea bed is

$$\phi^{(0)}(x, z) = B \exp(i\mu' d\hat{x}) \cosh \mu' d(\hat{z} + h/d), \tag{3.13}$$

where μ' is also an undetermined coefficient.

Applying the continuity of pressure and vertical component of velocity for (3.11) and (3.13) on the common fluid interface $\hat{z} = -1$ results in

$$\mu = \mu', \tag{3.14}$$

$$B \cosh \mu(h - d) = A(1 - Kd) \tag{3.15}$$

and

$$B\mu \sinh \mu(h - d) = AK. \tag{3.16}$$

That is, μ satisfies

$$\mu \tanh \mu(h - d) = K/(1 - Kd), \tag{3.17}$$

and the corresponding mode, written in terms of the original coordinates, is

$$\phi(x, z) = e^{i\mu x} \begin{cases} (1 + Kz)/(1 - Kd), & -d < z < 0, \\ \cosh \mu(h + z)/\cosh \mu(h - d), & -h < z < -d. \end{cases} \tag{3.18}$$

When $Kd \to 1$ we can see from (3.17) that $\mu d \to \infty$ and thus the assumption made in (3.11) that $\mu d \ll 1/\epsilon$ is violated.

In this section we have implemented a 'low-frequency homogenisation' and it can be expected to be valid if $|1 - Kd| \gg \epsilon$ which is also aligned with the assumption made in §2.4. The result (3.17) and (3.18) shows that the homogenisation of the boundary-value problem coincides with the small-δ/d limit (2.47) and (2.48) of the discrete barrier array problem with the association that $\beta \to \mu$ as $\delta/d \to 0$. Also, it can be proved that there

			$\delta/d = 0.05$			$\delta/d = 0.5$	
		$Kd = 0.2$	$Kd = 0.6$	$Kd = 1.0$	$Kd = 0.2$	$Kd = 0.6$	$Kd = 1.0$
	0	0.015009	0.075510	$\pi + 1.4309i$	0.15097	0.75208	$\pi + 1.4309i$
	2	0.014955	0.073792	$\pi + 2.1145i$	0.14596	0.64601	$\pi + 2.1145i$
M_1	4	0.014955	0.073782	$\pi + 2.1643i$	0.14594	0.64534	$\pi + 2.1643i$
	6	0.014955	0.073781	$\pi + 2.1683i$	0.14594	0.64527	$\pi + 2.1683i$
	8	0.014955	0.073781	$\pi + 2.1690i$	0.14594	0.64526	$\pi + 2.1690i$
	0	0.018245	—	—	0.15574	—	—
	2	0.015035	0.079583	—	0.14597	0.64793	$\pi + 3.9638i$
	4	0.014962	0.074119	—	0.14594	0.64528	$\pi + 2.2017i$
M_2	6	0.014956	0.073820	—	0.14594	0.64528	$\pi + 2.1702i$
	8	0.014955	0.073790	$\pi + 4.1211i$	0.14594	0.64528	$\pi + 2.1698i$
	10	0.014955	0.073786	$\pi + 2.6190i$	0.14594	0.64528	$\pi + 2.1698i$
	12	0.014955	0.073786	$\pi + 2.3200i$	0.14594	0.64528	$\pi + 2.1698i$

Table 1. The convergence of first non-dimensional Bloch wavenumber $\beta^{(0)}\delta$ against the truncation parameter, M_k, for the two schemes given in § 2.2 with $d/h = 0.2$. A dash (—) indicates cannot determine a value of β that makes the determinant zero.

exists one real value of μ_0 and a number of pure imaginary values of $\mu_n = i\hat{\mu}_n$ (where $n = 1, 2, \ldots$ and $\hat{\mu}_n \in ((n-1)\pi, n\pi)$) satisfying (3.17).

It should be possible to perform a 'high-frequency homogenisation' (see Craster, Kaplunov & Pichugin 2010) by expanding about the state $\beta\delta = \pi$ where a local standing mode exists and gives rise to the critical value of K_c below which wave propagation exists and above which wave propagation is prohibited.

3.1. *Results*

First, we determine the accuracy of the numerical scheme of § 2 by varying the truncation parameter, M_k ($k = 1, 2$), to assess the convergence of the two schemes given in § 2.2. Fundamental cells with the same submergence $d/h = 0.2$ but different spacings are considered in tables 1 and 2 which catalogue the numerical estimates of the first $\beta^{(0)}$ and second $\beta^{(1)}$ Bloch wavenumbers by solving each scheme. For the first Bloch wavenumber, when K exceeds a value of K_c corresponding to the critical frequency ω_c (where $K_c d < 1$), there no longer exists a real-valued Bloch wavenumber. Instead, following the system introduced in § 2, $\beta^{(0)}$ records a complex Bloch wavenumber and represents decay rather than wave propagation through the array. For the real value of $\beta^{(0)}$, when $M_k = 6$ the non-dimensional wavenumber $\beta^{(0)}\delta$ is determined to have nearly five-decimal-place accuracy except for the second scheme at relatively high frequencies. When the frequency exceeds the critical frequency, the larger truncation parameters are required for obtaining the first Bloch wavenumber with the same precision. As for the second Bloch wavenumber, the convergent results can be reached with very few terms. Generally, the first scheme tends to converge faster for small δ/d and the second scheme does better when δ/d takes larger values, the reason for which has been outlined earlier.

Next, we compare Bloch wavenumber $\beta^{(k)}$ obtained by (2.39) or (2.43) with numerical roots μ_k in the homogenisation method obtained by (3.17). Figure 1(a) shows the variation of the first value ($k = 0$) against the non-dimensional wavenumber Kd for submergence $d/h = 0.2$. As mentioned in § 2, real β are determined in the range of $\beta \in (0, \pi/\delta]$ and for the other ranges the problem is unchanged. Thus, in figure 1(a) the curves describing real Bloch wavenumbers terminate at $\beta = \pi/\delta$ and the value of $K_c d$ corresponding to

		$\delta/d = 0.05$			$\delta/d = 0.5$		
		$Kd = 0.2$	$Kd = 0.6$	$Kd = 1.0$	$Kd = 0.2$	$Kd = 0.6$	$Kd = 1.0$
	0	0.034974i	0.023387i	0.019611i	0.34854i	0.23080i	0.19394i
	1	0.034878i	0.023380i	0.019611i	0.33926i	0.23021i	0.19394i
M_1	2	0.034883i	0.023411i	0.019634i	0.34040i	0.23336i	0.19630i
	3	0.034883i	0.023411i	0.019634i	0.34040i	0.23335i	0.19630i
	4	0.034884i	0.023411i	0.019635i	0.34041i	0.23341i	0.19635i
	0	—	—	0.037744i	—	—	0.32364i
	1	—	0.024607i	0.019887i	0.39190i	0.24020i	0.19820i
M_2	2	0.034939i	0.023424i	0.019635i	0.34055i	0.23342i	0.19636i
	3	0.034932i	0.023416i	0.019635i	0.34042i	0.23342i	0.19636i
	4	0.034899i	0.023413i	0.019635i	0.34042i	0.23342i	0.19635i

Table 2. The convergence of second non-dimensional Bloch wavenumber $\beta^{(1)}\delta$ against the truncation parameter, M_k, for the two schemes given in § 2.2 with $d/h = 0.2$. A dash (—) indicates cannot determine a value of β that makes the determinant zero.
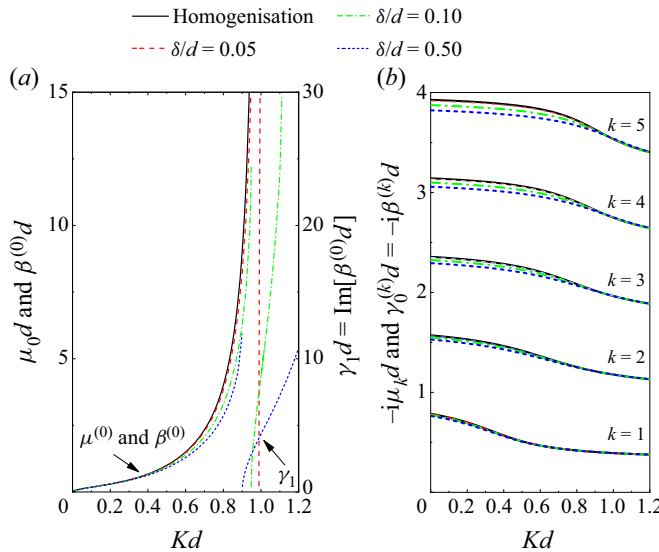

Figure 1. The variation of the roots μ_k from homogenisation and the Bloch–Floquet wavenumbers $\beta^{(k)}$ against the non-dimensional wavenumber Kd for a submergence $d/h = 0.2$: (a) the first value ($k = 0$); (b) the imaginary part of the first five pure imaginary values.

the critical frequencies in the figure shown are, respectively, 0.9891, 0.9477 and 0.9006. Above these critical frequencies, a complex value of $\beta = \pi/\delta + i\gamma_1$ emerges from the real axis, the imaginary part of which is also shown in figure 1(a). Thus, it can be inferred that when the frequency exceeds the critical frequency, the real Bloch–Floquet wavenumber will move off the real axis and go along the semi-infinite line $\beta = \pi/\delta + i\gamma_1$ for $\gamma_1 = [0, \infty)$. Besides, we can see that for small spacing, the complex solution increases extremely fast with frequency. Since the propagating mode no longer exists, we also can conclude that the first stop band during which wave propagation is prohibited is the interval $Kd \in (K_c d, (\pi d/\delta) \tanh(\pi h/\delta))$. The end points of this interval both correspond to $\beta\delta = \pi$ and standing waves occurring in the cell; the lower value corresponds to the case which is equivalent to a vertical baffle placed along the centreline of the cell, i.e. the
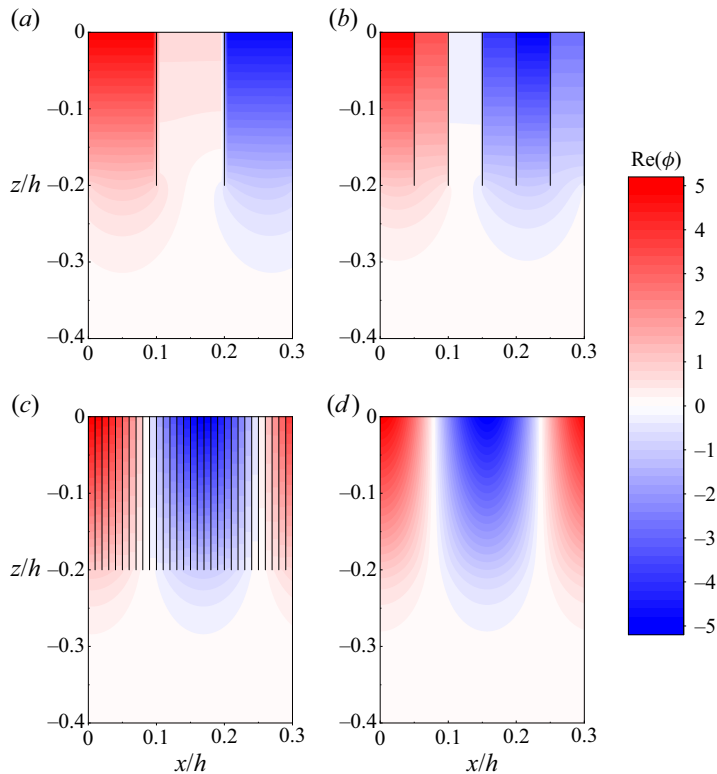
Figure 2. The fields of the real part of the velocity potential in the cell with the submergence $d/h = 0.2$ at $Kd = 0.8$: (a) $\delta/d = 0.50$; (b) $\delta/d = 0.25$; (c) $\delta/d = 0.05$; (d) homogenisation.

solution of (2.13), while the upper value corresponds the case in which barriers extend through the depth, i.e. the solution of (2.14). The real root, μ_0, of the dispersion equation (3.17) tends to infinity as $Kd \to 1$. The stop band under the homogenisation approximation is $Kd \in (1, \infty)$, i.e. the critical frequency $\omega_c = \sqrt{g/d}$ coinciding with Newman (1974) and representing resonance in narrow channels. Figure 1(b) plots the variation of the first five pure imaginary values. Generally, as the dimensionless spacing, δ/d, decreases β tends to μ as we have anticipated.

In figure 2, the velocity potential fields have been plotted in the range $0 < x/h < 0.3$ for a barrier submergence $d/h = 0.2$ at a non-dimensional wavenumber $Kd = 0.8$. In figure 2(a–c), the results correspond to $\beta^{(0)}$ and the barrier spacings are reduced from $\delta/d = 0.5$, to 0.25 and then to 0.05 so that we see 3, 6 and 30 cells respectively. It can be seen that oscillation within each channel is dominated by vertical fluid motion and as the channels decrease in width, the results tend towards the potential field obtained under homogenisation, shown in figure 2(d). Only the real part of the velocity potential is shown, but there is a similar agreement for the imaginary part.

In figure 3, we plot the fields of the velocity potential at $Kd = 0.9891$ where $\beta^{(0)}\delta = \pi$ for the case of $\delta/d = 0.05$ (the smallest spacing used in the previous plot). This is the case in which standing waves occur in the cell and the imaginary part of the velocity potential vanishes according to the Bloch–Floquet theory. The potentials are not normalised giving rise to large values in the plots. Unlike in figure 2, there is no longer good agreement between the Bloch–Floquet approach shown in figure 3(a) and homogenisation (the real
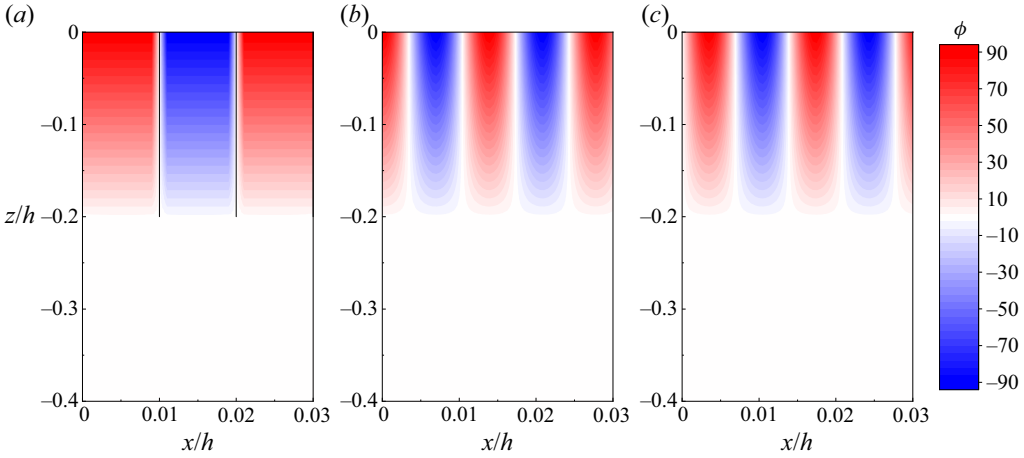
960 A20-16

Figure 3. Velocity potential field plots across $0 < x < 0.03$ with the submergence $d/h = 0.2$ at $Kd = 0.9891$: (a) $\delta/d = 0.05$ and $\beta^{(0)}\delta = \pi$; (b) homogenisation (real part); (c) homogenisation (imaginary part).

and imaginary parts of which are shown in figures 3b and 3c). This illustrates how homogenisation breaks down as an approximation to closely spaced discrete arrays as standing wave resonance is approached.

4. Scattering of incident waves by a finite periodic array of barriers

In this section, we consider the problem of $N + 1$ identical barriers each submerged to the same depth d and located at $x_n = n\delta$ for $n = 0, 1, \ldots, N$ as shown in figure 4, which is a finite section of the assumed infinite array given in § 2. Thus, the general solution in $(n - 1)\delta < x < n\delta$ can be expressed as a combination of the eigenfunctions $\phi^{(\pm k)}$ of the periodic Bloch–Floquet problem associated with $\beta = \pm\beta^{(k)}$:

$$\phi_n(x, z) = \sum_{k=0}^{\infty} \left[c_n^{(k)} \phi^{(+k)}(x - (n - 1)\delta, z) + d_n^{(k)} \phi^{(-k)}(x - (n - 1)\delta, z) \right], \qquad (4.1)$$

for $n = 1, 2, \ldots, N$. This representation of the solution was established in Porter & Porter (2003). It should be noted that since the local wave with a slow decay should be given priority for considering the oscillation in the barrier array, in this section a new labelling rule for $\beta^{(k)}$ is applied that $k = 0$ is prepared for the real eigenvalue if exists otherwise the complex eigenvalues of $\beta = n\pi/\delta + i\gamma_n$ ($n = 0, 1$) are ordered with their imaginary parts increasing, which is different from the labelling rule in § 2.

Continuity of pressure and velocity across the fluid interface under the barrier along $x = n\delta$ requires

$$\phi_{n+1}(n\delta, z) = \phi_n(n\delta, z) \quad \text{and} \quad \frac{\partial \phi_{n+1}}{\partial x}(n\delta, z) = \frac{\partial \phi_n}{\partial x}(n\delta, z), \qquad (4.2a,b)$$

for $-h < z < -d$ and $n = 1, 2, \ldots, N - 1$. Using the orthogonality relation (2.11) derived earlier in § 2.1, we find that

$$c_{n+1}^{(j)} E^{(+j)} = \int_{-h}^{d} \left[\phi_{n+1}(n\delta, z) \frac{\partial \phi^{(-j)}}{\partial x}(0, z) - \phi^{(-j)}(0, z) \frac{\partial \phi_{n+1}}{\partial x}(n\delta, z) \right] dz \qquad (4.3)$$
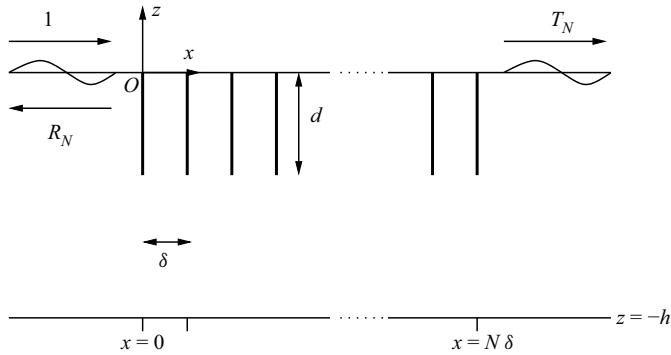
960 A20-17

Figure 4. An illustration of scattering by a finite periodic array of $N + 1$ identical surface-piercing barriers.

and

$$d_{n+1}^{(j)} E^{(-j)} = \int_{-h}^{d} \left[\phi_{n+1}(n\delta, z) \frac{\partial \phi^{(+j)}}{\partial x}(0, z) - \phi^{(+j)}(0, z) \frac{\partial \phi_{n+1}}{\partial x}(n\delta, z) \right] dz. \qquad (4.4)$$

Using the matching conditions (4.2a,b) and the definition (4.3) gives

$$c_{n+1}^{(j)} E^{(+j)} = \int_{-h}^{d} \left[\phi_n(n\delta, z) \frac{\partial \phi^{(-j)}}{\partial x}(0, z) - \phi^{(-j)}(0, z) \frac{\partial \phi_n}{\partial x}(n\delta, z) \right]_{x=0} dz$$

$$= c_n^{(j)} E^{(+j)} \exp(+i\beta^{(j)}\delta), \qquad (4.5)$$

after using the phase relations (2.5) for the jth eigenfunction to transfer information from $x = \delta$ to $x = 0$ and the orthogonality relation (2.11) again. We do the same for $d_n^{(j)}$ allowing us to deduce that

$$c_{n+1}^{(j)} = \exp(+i\beta^{(j)}\delta)c_n^{(j)} \quad \text{and} \quad d_{n+1}^{(j)} = \exp(-i\beta^{(j)}\delta)d_n^{(j)}. \qquad (4.6a,b)$$

That is, there is no coupling between eigenmodes as waves propagate through the periodic array having the consequence that

$$c_N^{(j)} = \exp(i\beta^{(j)}(N - 1)\delta)c_1^{(j)} \quad \text{and} \quad d_N^{(j)} = \exp(-i\beta^{(j)}(N - 1)\delta)d_1^{(j)}. \qquad (4.7a,b)$$

In other words, if the solution in $0 < x < \delta$ is expressed as

$$\phi_1(x, z) = \sum_{k=0}^{\infty} \left[c_1^{(k)} \phi^{(+k)}(x, z) + d_1^{(k)} \phi^{(-k)}(x, z) \right], \qquad (4.8)$$

then the general solution across the whole barrier array domain $0 < x < N\delta$ is represented in terms of just one set of expansion coefficients, $c_1^{(k)}$ and $d_1^{(k)}$. In particular, the solution in $(N - 1)\delta < x < N\delta$ is

$$\phi_N(x, z) = \sum_{k=0}^{\infty} [c_1^{(k)} \exp(i\beta^{(k)}(N - 1)\delta)\phi^{(+k)}(x - (N - 1)\delta, z)$$

$$+ d_1^{(k)} \exp(-i\beta^{(k)}(N - 1)\delta)\phi^{(-k)}(x - (N - 1)\delta, z)]. \qquad (4.9)$$

The scattering problem involves waves incident from and reflected into the domain $\{x < 0, -h < z < 0\}$ in which the general solution is represented by the standard expansion

960 A20-18

(e.g. Linton & McIver 2001)

$$\phi_0(x, z) = (e^{ikx} + R_N \exp(-ikx))\psi_0(z) + \sum_{n=1}^{\infty} a_n e^{k_n x}\psi_n(z), \quad (4.10)$$

where R_N is the reflection coefficient, a_n (and, later, b_n) are expansion coefficients and $\psi_n(z)$ is the vertical eigenfunction which has been given in (2.27). It helps to write (4.10) as

$$\phi_0(x, z) = 2\cos kx \psi_0(z) + \sum_{n=0}^{\infty} a_n e^{k_n x}\psi_n(z), \quad (4.11)$$

where $R_N = 1 + a_0$. In $x > N\delta$, waves are transmitted and the general solution is represented by

$$\phi_{N+1}(x, z) = \sum_{n=0}^{\infty} b_n \exp(-k_n(x - N\delta))\psi_n(z), \quad (4.12)$$

with transmission coefficient $T_N = b_0 \exp(-ikN\delta)$.

With (4.8) holding in the region adjoining $x = 0$ and (4.9) holding in the region adjoining $x = N\delta$, the remaining conditions that need to be enforced in order to determine the values of a_n, b_n for $n = 0, 1, \ldots$ and $c_1^{(k)}$, $d_1^{(k)}$ for $k = 0, 1, \ldots$ are

$$\frac{\partial \phi_0}{\partial x}(0, z) = 0 \quad \text{and} \quad \frac{\partial \phi_{N+1}}{\partial x}(N\delta, z) = 0, \quad (4.13a,b)$$

for $-d < z < 0$, and

$$\phi_0(0, z) = \phi_1(0, z) \quad \text{and} \quad \phi_N(N\delta, z) = \phi_{N+1}(N\delta, z), \quad (4.14a,b)$$

$$\frac{\partial \phi_0}{\partial x}(0, z) = \frac{\partial \phi_1}{\partial x}(0, z) \equiv U(z) \quad \text{and} \quad \frac{\partial \phi_N}{\partial x}(N\delta, z) = \frac{\partial \phi_{N+1}}{\partial x}(N\delta, z) \equiv V(z), \quad (4.15a,b)$$

for $-h < z < -d$. Applying the condition (4.15a,b) to (4.11) and (4.12) and the orthogonality of the vertical eigenfunctions (2.29) results in

$$\phi_0(x, z) = 2\cos kx \psi_0(z) + \sum_{n=0}^{\infty} \frac{\psi_n(z) e^{k_n x}}{k_n h} \int_{-h}^{-d} U(z')\psi_n(z') \, dz' \quad (4.16)$$

in $x < 0$ and

$$\phi_{N+1}(x, z) = -\sum_{n=0}^{\infty} \frac{\psi_n(z) \exp(-k_n(x - N\delta))}{k_n h} \int_{-h}^{-d} V(z')\psi_n(z') \, dz' \quad (4.17)$$

in $x > N\delta$. It also follows that

$$R_N = 1 + \frac{i}{kh} \int_{-h}^{-d} U(z)\psi_0(z) \, dz \quad \text{and} \quad T_N = -\frac{i \exp(-ikN\delta)}{kh} \int_{-h}^{-d} V(z)\psi_0(z) \, dz. \quad (4.18a,b)$$

The matching across $x = 0$ and $x = N\delta$ requires some work since the representation of the solution in $x < 0$ and $x > N\delta$ in terms of eigenfunctions in z is fundamentally different

from the representation of the solution in $0 < x < N\delta$ which is based on Bloch–Floquet eigenmodes. We start by using (4.3) and (4.4) with $n = 0$ to give

$$
\begin{aligned}
c_1^{(j)} E^{(+j)} &= \int_{-h}^{-d} \left[\phi_1(0, z) \frac{\partial \phi^{(-j)}}{\partial x}(0, z) - \phi^{(-j)}(0, z) \frac{\partial \phi_1}{\partial x}(0, z) \right] \mathrm{d}z \\
&= \int_{-h}^{-d} \left[\phi_0(0, z) \frac{\partial \phi^{(-j)}}{\partial x}(0, z) - \phi^{(-j)}(0, z) U(z) \right] \mathrm{d}z
\end{aligned}
\tag{4.19}
$$

and

$$
\begin{aligned}
d_1^{(j)} E^{(-j)} &= \int_{-h}^{-d} \left[\phi_1(0, z) \frac{\partial \phi^{(+j)}}{\partial x}(0, z) - \phi^{(+j)}(0, z) \frac{\partial \phi_1}{\partial x}(0, z) \right] \mathrm{d}z \\
&= \int_{-h}^{-d} \left[\phi_0(0, z) \frac{\partial \phi^{(+j)}}{\partial x}(0, z) - \phi^{(+j)}(0, z) U(z) \right] \mathrm{d}z,
\end{aligned}
\tag{4.20}
$$

where the matching conditions (4.14*a,b*) and (4.15*a,b*) have been applied. On account of the relations (2.7) and (2.8) and using (4.16), we can rewrite (4.19) and (4.20) as

$$
\begin{aligned}
c_1^{(j)} \exp(-\mathrm{i}\beta^{(j)}\delta) E^{(+j)} &= -2H_{j0} - \sum_{n=0}^{\infty} \frac{H_{jn}}{k_n h} \int_{-h}^{-d} U(z') \psi_n(z') \, \mathrm{d}z' \\
&\quad - \int_{-h}^{-d} \phi^{(+j)}(0, z) U(z) \, \mathrm{d}z
\end{aligned}
\tag{4.21}
$$

and

$$
d_1^{(j)} E^{(-j)} = 2H_{j0} + \sum_{n=0}^{\infty} \frac{H_{jn}}{k_n h} \int_{-h}^{-d} U(z') \psi_n(z') \, \mathrm{d}z' - \int_{-h}^{-d} \phi^{(+j)}(0, z) U(z) \, \mathrm{d}z,
\tag{4.22}
$$

where

$$
H_{jn} = \int_{-h}^{-d} \frac{\partial \phi^{(+j)}}{\partial x}(0, z) \psi_n(z) \, \mathrm{d}z.
\tag{4.23}
$$

Using (4.5) with $n = N$ and following the same procedure give

$$
c_1^{(j)} \exp(\mathrm{i}\beta^{(j)}(N-1)\delta) E^{(+j)} = \sum_{n=0}^{\infty} \frac{H_{jn}}{k_n h} \int_{-h}^{-d} V(z') \psi_n(z') \, \mathrm{d}z' - \int_{-h}^{-d} \phi^{(+j)}(0, z) V(z) \, \mathrm{d}z
\tag{4.24}
$$

and

$$
d_1^{(j)} \exp(-\mathrm{i}\beta^{(j)} N\delta) E^{(-j)} = -\sum_{n=0}^{\infty} \frac{H_{jn}}{k_n h} \int_{-h}^{-d} V(z') \psi_n(z') \, \mathrm{d}z' - \int_{-h}^{-d} \phi^{(+j)}(0, z) V(z) \, \mathrm{d}z.
\tag{4.25}
$$

The algebraic manipulations above allow us to express the coefficients $c_1^{(j)}$ and $d_1^{(j)}$, and hence the solutions ϕ_1 and ϕ_N in $0 < x < \delta$ and $(N-1)\delta < x < N\delta$ (respectively) are

960 A20-20

in terms of the unknown functions $U(z)$ and $V(z)$. This replicates what we had already achieved in (4.16) and (4.17) for ϕ_0 and ϕ_{N+1} in $x < 0$ and $x > N\delta$.

Eliminating $c_1^{(j)}$ in (4.21) and (4.24) eventually results in

$$\int_{-h}^{-d} U(z)\mathcal{K}_j^{(1)}(z)\,\mathrm{d}z + \int_{-h}^{-d} V(z)\mathcal{K}_j^{(2)}(z)\,\mathrm{d}z = -2\exp(\mathrm{i}\beta^{(j)}N\delta)H_{j0}, \tag{4.26}$$

where

$$\mathcal{K}_j^{(1)}(z) = \exp(\mathrm{i}\beta^{(j)}N\delta)\left[\sum_{n=0}^{\infty} \frac{H_{jn}}{k_n h}\psi_n(z) + \phi^{(+j)}(0, z)\right] \tag{4.27}$$

and

$$\mathcal{K}_j^{(2)}(z) = \sum_{n=0}^{\infty} \frac{H_{jn}}{k_n h}\psi_n(z) - \phi^{(+j)}(0, z). \tag{4.28}$$

Also eliminating $d_1^{(j)}$ in (4.22) and (4.25) gives

$$\int_{-h}^{-d} U(z)\mathcal{K}_j^{(2)}(z)\,\mathrm{d}z + \int_{-h}^{-d} V(z)\mathcal{K}_j^{(1)}(z)\,\mathrm{d}z = -2H_{j0}. \tag{4.29}$$

We note that if we write

$$U^s(z) = U(z) + V(z) \quad \text{and} \quad U^a(z) = U(z) - V(z), \tag{4.30a,b}$$

then (4.26) and (4.29) decouple into a pair of scalar integral equations:

$$\int_{-h}^{-d} U^{s,a}(z)\mathcal{K}_j^{s,a}(z)\,\mathrm{d}z = -2H_{j0}, \tag{4.31}$$

where

$$\begin{aligned}\mathcal{K}_j^s(z) &= \frac{1}{\exp(\mathrm{i}\beta^{(j)}N\delta) + 1}\left[\mathcal{K}_j^{(1)}(z) + \mathcal{K}_j^{(2)}(z)\right] \\ &= \sum_{n=0}^{\infty} \frac{H_{jn}}{k_n h}\psi_n(z) + \mathrm{i}\tan\left(\beta^{(j)}N\delta/2\right)\phi^{(+j)}(0, z)\end{aligned} \tag{4.32}$$

and

$$\begin{aligned}\mathcal{K}_j^a(z) &= \frac{1}{\exp(\mathrm{i}\beta^{(j)}N\delta) - 1}\left[\mathcal{K}_j^{(1)}(z) - \mathcal{K}_j^{(2)}(z)\right] \\ &= \sum_{n=0}^{\infty} \frac{H_{jn}}{k_n h}\psi_n(z) - \mathrm{i}\cot\left(\beta^{(j)}N\delta/2\right)\phi^{(+j)}(0, z).\end{aligned} \tag{4.33}$$

The use of superscripts s and a indicates that the two integral equations can be thought of as representing the components of the scattering by the barrier array which are symmetric and antisymmetric about the mid-plane, $x = N\delta/2$, of geometric symmetry.

4.1. *Numerical approximation*

The pair of integral equations (4.31) is approximated numerically using the identical method in § 2.3. Thus the two functions $U^s(z)$ and $U^a(z)$ have the same form as (2.41):

$$U^{s,a}(z) \approx \sum_{n=0}^{M} \alpha_n^{s,a} u_n(z), \tag{4.34}$$

where $u_n(z)$ are defined in (2.42).

After substituting (4.34) into (4.31) we can obtain the following systems of equations:

$$\sum_{n=0}^{M} \alpha_n^{s,a} K_{mn}^{s,a} = -2H_{m0}, \tag{4.35}$$

for $m = 0, 1, \ldots, M$, where

$$K_{mn}^s = \sum_{r=0}^{\infty} \frac{H_{mr}F_{nr}}{k_r h} + \mathrm{i}\tan\left(\beta^{(m)} N\delta/2\right) G_{mn} \tag{4.36}$$

and

$$K_{mn}^a = \sum_{r=0}^{\infty} \frac{H_{mr}F_{nr}}{k_r h} - \mathrm{i}\cot\left(\beta^{(m)} N\delta/2\right) G_{mn}, \tag{4.37}$$

in which F_{mr} have already been defined in (2.45) and

$$G_{mn} = \int_{-h}^{-d} u_n(z)\phi^{(+m)}(0, z)\,\mathrm{d}z. \tag{4.38}$$

The system of equations (4.35) has been truncated with the parameter M which need not be the same as M_k in § 2.3. From (4.34) we can see that M denotes the number of the vertical eigenfunctions used to approximate the horizontal velocity on the interface; on the other hand, from (4.36), (4.37) and (4.38) we can see that M also represents the number of the evanescent modes applied to simulate the oscillation in the barrier array.

In the Bloch–Floquet problem, two solutions of $\phi^{(+m)}(0, z)$ in different forms are presented in § 2 such that the eigenfunctions can be approximated by either (2.17) or (2.25) resulting in that G_{mn} can be written as

$$G_{mn} = \sum_{l=-\infty}^{\infty} \frac{(-1)^n b_{1,l}^{(m)}}{\cosh\beta_l^{(m)}(h-d)} I_{2m}\left[\beta_l^{(m)}(h-d)\right] \tag{4.39}$$

or

$$G_{mn} = \sum_{l=0}^{\infty} \left(a_{2,l}^{(m)} + b_{2,l}^{(m)}\right) F_{nl}. \tag{4.40}$$

The series in G_{mn} decays like $O(1/l^2)$ as l tends to infinity, which can be treated with the same procedure shown in Appendix A. However, for H_{mr} in (4.23) we find that either solution will produce a slowly convergent series decreasing like $O(1/l^{3/2})$ if the expressions of $\phi^{(+m)}(0, z)$ are applied directly. In order to calculate H_{mr} efficiently, we

960 A20-22

use the approximation in (2.30) which is based on the second form in § 2. Then, H_{mr} can be written as

$$H_{mr} = \sum_{k=0}^{M_2} \alpha_{2,k}^{(m)} F_{kr} \tag{4.41}$$

after using (2.41), where $\alpha_{2,k}^{(m)}$ are eigenvectors corresponding to the eigenvalue $\beta^{(m)}$. Now a slowly convergent infinite series is replaced with a truncated series such that the series in (4.36) and (4.37) decaying like $O(1/r^2)$ also can be computed efficiently if the method in Appendix A is used.

Once $\alpha_n^{s,a}$ have been determined from (4.35), we can recover the reflection and transmission coefficients from the use of (4.30a,b) in (4.18a,b) with (4.34) and (2.45) to give

$$R_N = 1 + \frac{i}{2kh} \sum_{n=0}^{M} (\alpha_n^s + \alpha_n^a) F_{m0} \quad \text{and} \quad T_N = -\frac{i \exp(-ikN\delta)}{2kh} \sum_{n=0}^{M} (\alpha_n^s - \alpha_n^a) F_{m0}. \tag{4.42a,b}$$

Combined with the description in § 2.3, it can be seen that the two different forms of eigenfunction $\phi^{(\pm m)}(x, z)$ have their own advantages. The first form is better for approximating solutions to the Bloch–Floquet problem, especially for closely spaced barriers and the explicit limit of vanishing spacing can be taken. On the other hand, with the help of the second form, the slowly convergent series appearing in the scattering problem for a finite periodic array can be treated efficiently. In addition, from (4.36) and (4.37) we also can see that the present method has the same advantages as the recursive transfer matrix method (e.g. Porter & Porter 2003) in that the dimension of the equation system is independent of the size of the array.

Furthermore, it should be noted that the reflection and transmission coefficients (4.42a,b) cannot be applied for the case of the critical frequency (i.e. $\beta^{(0)} = \pi/\delta$) since the eigenfunctions $\phi^{(\pm 0)}$ no longer satisfy the orthogonality relation (2.11) which has been widely used in the above derivation.

5. Scattering using the continuum model

Consider that the region $0 < x < N\delta$ is governed by the continuum model described in § 3, so that the potential in this region may be written as

$$\phi_h(x, z) = \sum_{n=0}^{\infty} (c_n \exp(i\mu_n x) + d_n \exp(i\mu_n(N\delta - x))) Z_n(z), \tag{5.1}$$

where

$$Z_n(z) = \varepsilon_n^{-1/2} \begin{cases} (1 + Kz)/(1 - Kd), & -d < z < 0, \\ \cosh \mu_n(h + z)/\cosh \mu_n(h - d), & -h < z < -d, \end{cases} \tag{5.2}$$

and μ_n are the roots of (3.17). Also, in this section a new labelling rule is used for μ_n that the real value takes precedence over increasing pure imaginary values and if there does not exist the real value the smallest value on the imaginary axis takes $\mu^{(0)}$. In (5.2), ε_n are

normalisation factors given by

$$\varepsilon_n = \frac{1}{2\cosh^2 \mu_n(h-d)} \left[1 + \frac{\sinh 2\mu_n(h-d)}{2\mu_n(h-d)} \right], \tag{5.3}$$

so that

$$\frac{1}{h-d} \int_{-h}^{-d} Z_n(z) Z_m(z) \, dz = \delta_{mn}. \tag{5.4}$$

This orthogonality relation for the functions $Z_n(z)$ follows since μ_n are distinct and

$$(\mu_n^2 - \mu_m^2) \int_{-h}^{-d} Z_n(z) Z_m(z) dz = \int_{-h}^{-d} \left[Z_n''(z) Z_m(z) - Z_n(z) Z_m''(z) \right] dz$$

$$= \left[Z_n'(z) Z_m(z) - Z_n(z) Z_m'(z) \right]_{-h}^{-d} = 0, \tag{5.5}$$

where the dispersion relation (3.17) has been used.

The matching conditions shown in (4.13*a,b*), (4.14*a,b*) and (4.15*a,b*) still hold but ϕ_h will replace ϕ_1 and ϕ_N. Continuity of the horizontal velocity at $x = 0$ and $x = N\delta$ results in

$$c_n - d_n \exp(i\mu_n N\delta) = \frac{1}{i\mu_n(h-d)} \int_{-h}^{-d} U(z) Z_n(z) \, dz \tag{5.6}$$

and

$$c_n \exp(i\mu_n N\delta) - d_n = \frac{1}{i\mu_n(h-d)} \int_{-h}^{-d} V(z) Z_n(z) \, dz. \tag{5.7}$$

This gives

$$c_n = \frac{1}{2\mu_n(h-d)\sin\mu_n N\delta} \int_{-h}^{-d} \left[U(z)\exp(-i\mu_n N\delta) - V(z) \right] Z_n(z) \, dz \tag{5.8}$$

and

$$d_n = \frac{1}{2\mu_n(h-d)\sin\mu_n N\delta} \int_{-h}^{-d} \left[U(z) - V(z)\exp(-i\mu_n N\delta) \right] Z_n(z) \, dz. \tag{5.9}$$

Matching (5.1) to (4.16) across $x = 0$ gives

$$\int_{-h}^{-d} U(z') \mathcal{L}^{(1)}(z, z') \, dz' + \int_{-h}^{-d} V(z') \mathcal{L}^{(2)}(z, z') \, dz' = -2\psi_0(z) \tag{5.10}$$

and to (4.17) across $x = N\delta$ gives

$$\int_{-h}^{-d} U(z') \mathcal{L}^{(2)}(z, z') \, dz' + \int_{-h}^{-d} V(z') \mathcal{L}^{(1)}(z, z') \, dz' = 0, \tag{5.11}$$

where

$$\mathcal{L}^{(1)}(z, z') = \sum_{n=0}^{\infty} \left[\frac{\psi_n(z)\psi_n(z')}{k_n h} - \frac{Z_n(z) Z_n(z')}{\mu_n(h-d)\tan(\mu_n N\delta)} \right] \tag{5.12}$$

and

$$\mathcal{L}^{(2)}(z, z') = \sum_{n=0}^{\infty} \frac{Z_n(z) Z_n(z')}{\mu_n(h-d)\sin(\mu_n N\delta)}. \tag{5.13}$$

960 A20-24

For (5.10) and (5.11), we also can decouple the pair of integral equations into their symmetric and antisymmetric components like (4.30*a,b*) which satisfy

$$\int_{-h}^{-d} U^{s,a}(z')\mathcal{L}^{(s,a)}(z, z')\,\mathrm{d}z' = -2\psi_0(z), \tag{5.14}$$

where

$$\mathcal{L}^{(s)}(z, z') = \mathcal{L}^{(1)}(z, z') + \mathcal{L}^{(2)}(z, z')$$
$$= \sum_{n=0}^{\infty} \left[\frac{\psi_n(z)\psi_n(z')}{k_n h} + \frac{\tan(\mu_n N\delta/2)}{\mu_n(h - d)} Z_n(z)Z_n(z') \right] \tag{5.15}$$

and

$$\mathcal{L}^{(a)}(z, z') = \mathcal{L}^{(1)}(z, z') - \mathcal{L}^{(2)}(z, z')$$
$$= \sum_{n=0}^{\infty} \left[\frac{\psi_n(z)\psi_n(z')}{k_n h} - \frac{\cot(\mu_n N\delta/2)}{\mu_n(h - d)} Z_n(z)Z_n(z') \right]. \tag{5.16}$$

These are the equations that would be derived had the original problem been decomposed into the sum of problems symmetric and antisymmetric about the mid-plane $x = N\delta/2$.

5.1. *Numerical approximation*

The approximation (4.34) will be used again. We substitute (4.34) into (5.12), multiply through by $u_m(z)$ and integrate over $-h < z < -d$, a process which characterises the Galerkin method and results in the following systems of equations:

$$\sum_{n=0}^{M} \alpha_n^{s,a} L_{mn}^{s,a} = -2F_{m0}, \tag{5.17}$$

for $m = 0, 1, \ldots, M$, where

$$L_{mn}^s = \sum_{r=0}^{\infty} \frac{F_{mr}F_{nr}}{k_r h} + \sum_{r=0}^{\infty} \frac{\tan(\mu_r N\delta/2)}{\mu_r(h - d)} P_{mr}P_{nr} \tag{5.18}$$

and

$$L_{mn}^a = \sum_{r=0}^{\infty} \frac{F_{mr}F_{nr}}{k_r h} - \sum_{r=0}^{\infty} \frac{\cot(\mu_r N\delta/2)}{\mu_r(h - d)} P_{mr}P_{nr}, \tag{5.19}$$

in which

$$P_{mr} = \int_{-h}^{-d} u_m(z)Z_r(z)\,\mathrm{d}z = \varepsilon_m^{-1/2}(-1)^m I_{2m}[\mu_r(h - d)]. \tag{5.20}$$

All of the series in (5.18) and (5.19) have the order of $O(1/r^2)$ when $r \to \infty$, so the treatment shown in Appendix A can be applied to accelerate the series convergence. After the systems of equations are solved numerically, the reflection and transmission coefficients can be determined also by (4.42*a,b*).

It can be seen that the derivation for the reflection and transmission coefficients between the discrete model and the continuum model is different. For the discrete model, the

	$\delta/d = 0.05$			$\delta/d = 0.5$			Homogenisation	
M	$Kd = 0.2$	$Kd = 0.6$	$Kd = 1.0$	$Kd = 0.2$	$Kd = 0.6$	$Kd = 1.0$	$Kd = 0.2$	$Kd = 0.6$
0	0.20255	0.43354	0.99999	0.18198	0.57391	0.99998	0.22246	0.59119
4	0.19816	0.62013	1.00000	0.17969	0.64652	1.00000	0.19975	0.58320
8	0.19802	0.61743	1.00000	0.17969	0.64648	1.00000	0.19980	0.58450
12	0.19801	0.61711	1.00000	0.17969	0.64647	1.00000	0.19980	0.58467
16	0.19800	0.61694	1.00000	0.17969	0.64647	1.00000	0.19980	0.58471

Table 3. The convergence of the modulus of reflection coefficient $|R_N|$ computed using the discrete model and the continuum model against the truncation parameter, M, in the case of $d/h = 0.2$ and $N\delta = h$.

number of the truncated evanescent mode M is equal to the dimension of the equation system (see (4.35)). As shown later, $M = 12$ is usually sufficient to obtain convergent results. For the continuum model, the evanescent mode is included in the series shown in (5.18) and (5.19). We generally need to consider roughly 1000 terms to guarantee the accuracy of the series calculation. Actually, for the continuum model, we also can develop a system of equations similar to (4.35). However, we find that this would present a troublesome series when close to the critical frequency.

5.2. *Results*

We first examine the convergence of the scheme for the discrete model and the continuum model. In both settings, the barriers are submerged to a depth $d/h = 0.2$ and the total distribution length of the barriers is $N\delta = h$. Table 3 shows how the modulus of the reflection coefficient, $|R_N|$, converges with the truncation parameter, M. At low frequencies, results can be seen to converge quickly requiring only a small system of equations, but when the frequency approaches the critical frequency results tend to converge slowly with M since the amplitude of the fluid oscillation in the barrier array structure becomes increasingly severe. When the frequency is in the stop band, the wave motion decays through the array and there is practically no transmission. As mentioned at the end of § 4.1, the second method in § 2, which tends to converge fastest when δ/d is larger, is used in this scattering problem for determining the slowly convergent series. Thus, for the discrete model, the convergent results for distribution with large spacing can be obtained by a small truncation parameter used. In general, $M = 12$ is sufficient to produce results with the accuracy of roughly four significant figures although computations are more demanding when close to the critical frequency.

Next, some cases have been chosen to allow the comparison between the discrete model based on an expansion in terms of Bloch–Floquet eigenfunctions and existing results. A pair of barriers ($N = 1$) with the submergence $d/h = 0.2$ is first examined for which Porter & Evans (1995) previously provided accurate computations using the Galerkin approximation method. As shown in figure 5, the results of the discrete model compare favourably with these existing results, accurately replicating total reflection and transmission. Notice that the heavily suppressed transmission beyond $Kd \approx 1$ can now be understood as being associated with the stop band for the periodic barrier array despite there only being two barriers and one cell in the present example.

When the number of barriers $N + 1$ is large, direct solution methods such as those used by Porter & Evans (1995) are algebraically cumbersome and lead to $N + 1$ coupled equations in terms of $N + 1$ unknown functions eventually implying that numerical computations are of $O(N^3)$. To mitigate against this, previous authors
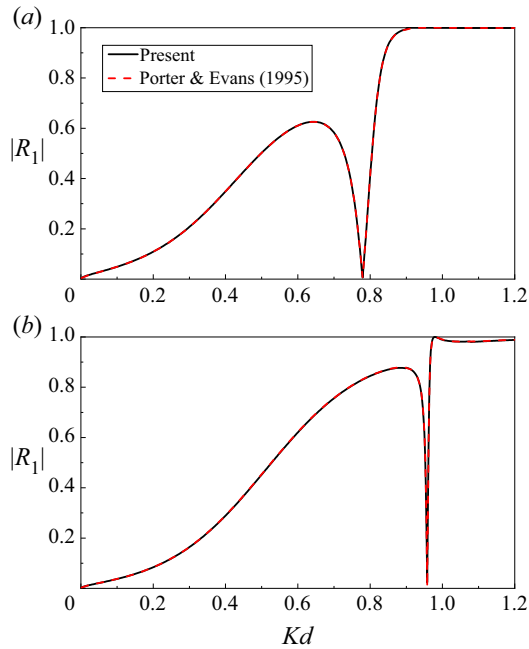
Figure 5. Comparison of the modulus of the reflection coefficient $|R_1|$ for the discrete model with existing results (Porter & Evans 1995) for the case of $N = 1$ and $d/h = 0.2$: (*a*) $\delta/d = 0.50$; (*b*) $\delta/d = 0.05$.

(e.g. Porter & Porter 2003) have used transfer matrices in which the scattering by $N + 1$ elements of the array is accounted for by the multiplication of $N + 1$ matrices whose size depends on the number of evanescent wave interactions retained in the exchange of information between adjacent elements in the array. Superficially the computational effort is of $O(N)$. In figure 6, we fix the number of barriers $N = 10$ and the submergence $d/h = 0.2$ and compare the modulus of the reflection coefficient $|R_{10}|$ computed using the present Bloch–Floquet discrete model (which does not scale with N) with those computed using transfer matrices. The results agree well, apart from when very close to the critical frequency where resonance occurs and when N is large. On account of the high-frequency oscillations in $|R_N|$ close to the critical frequency, even small errors in either the transfer matrix method or the present approach can lead to large changes in $|R_N|$ and it is not easy to determine which is more accurate. In particular, as the spacing decreases an increasing number of evanescent modes is required to maintain accurate computations resulting in larger transfer matrices and, in turn, this leads to numerical instability caused by rounding errors even though a treatment for avoiding these rounding errors devised by Porter & Porter (2003) has been applied. Thus, for the case of $\delta/d = 0.05$, the calculation by the method of the transfer matrix fails and figure 6(*c*) only includes the results from the present discrete model. During the review of this paper, one of the reviewers pointed out that the method devised by Ko & Sambles (1988) may be used to overcome the numerical instability issues caused by using transfer matrices.

As mentioned in the Introduction, one aim of the present study is to assess the validity of the homogenisation method for wave interaction with plate array structures. We first investigate the validity of the homogenisation method by varying the number of barriers (or the total length of the barrier array). In figure 7, the case of $\delta/d = 0.05$ and $d/h = 0.2$ is investigated with $N = 1$, $N = 5$ and $N = 10$ and results from the exact discrete model are plotted against the results from the homogenisation approximation. We recall that
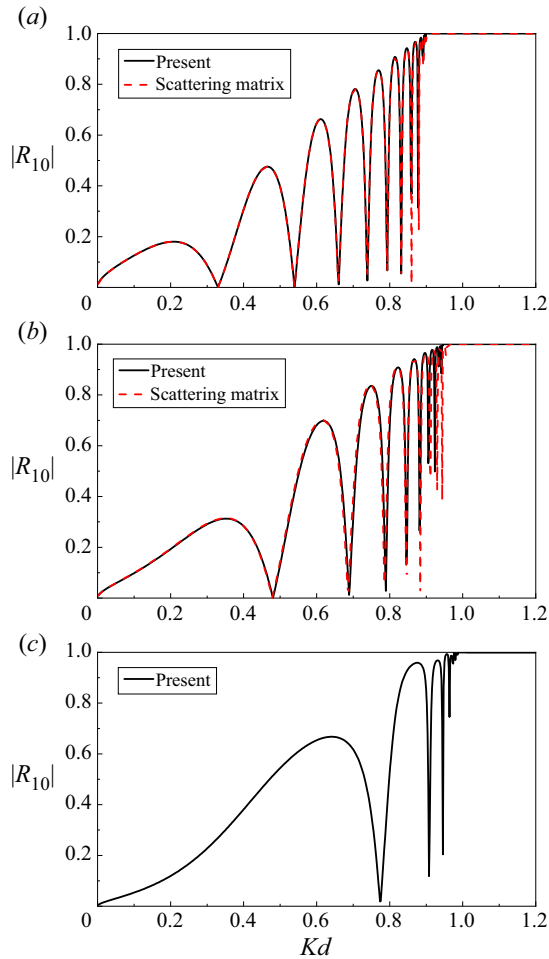
Figure 6. Comparison of the modulus of the reflection coefficient $|R_{10}|$ for the discrete model with the scattering matrix for the case of $N = 10$ and $d/h = 0.2$: (*a*) $\delta/d = 0.50$; (*b*) $\delta/d = 0.25$; (*c*) $\delta/d = 0.05$.

homogenisation is not expected to work for Kd sufficiently close to a value of $K_c d = 1$ corresponding to the critical frequency and curves will oscillate infinitely quickly as $Kd = 1$ is approached. On the other hand, the curves of $|R_N|$ computed under the discrete model oscillate and the total transmission will happen N times before the critical frequency is reached. Thus, we see in figure 7 overall good agreement between the exact and approximate models apart from close to $Kd = 1$.

In figure 8 we present the modulus of the reflection coefficient $|R_N|$ for the discrete model and the continuum model. The total length of the barrier array is fixed (i.e. $N\delta = h$), but the spacing in different arrays varies. This plot allows us to see how scattering computed from the discrete model converges to the results predicted from homogenisation. Again the submergence is $d/h = 0.2$ (the depth of the fluid is relatively unimportant for the effects we are observing). The spacing $\delta/d = 0.5$ corresponds to $N = 10$ whilst $\delta/d = 0.05$ corresponds to $N = 50$. The two curves corresponding to these two cases hit the horizontal axis (i.e. $|R_N| = 0$) 10 and 50 times respectively (although this cannot be captured by the resolution in the plots). We can see the agreement is good for low frequencies and gets better as δ/d decreases, although the rapid oscillations in $|R_N|$,
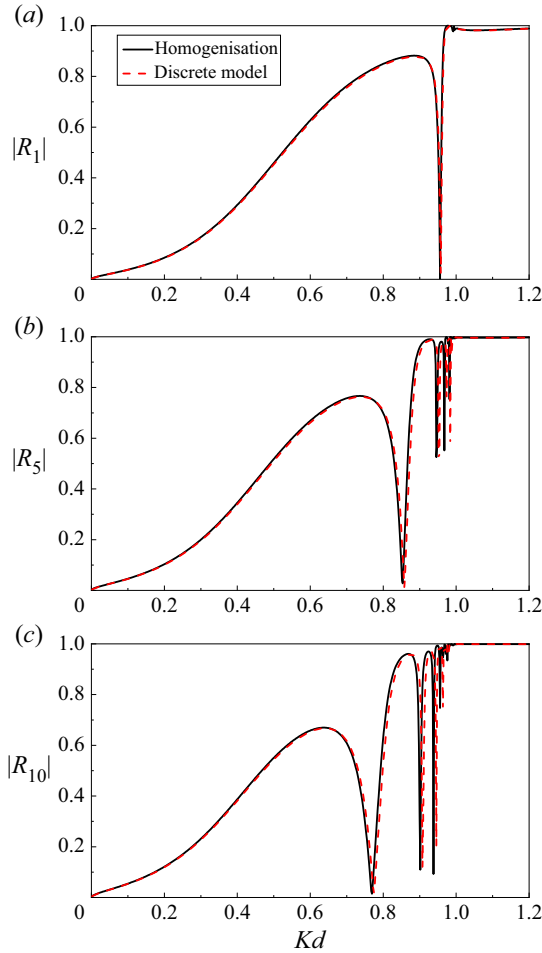
960 A20-28

Figure 7. The variation of the modulus of reflection coefficient $|R_N|$ for the discrete model and the continuum model against the non-dimensional frequency Kd for the case of $\delta/d = 0.05$ and $d/h = 0.2$: (a) $N = 1$; (b) $N = 5$; (c) $N = 10$.
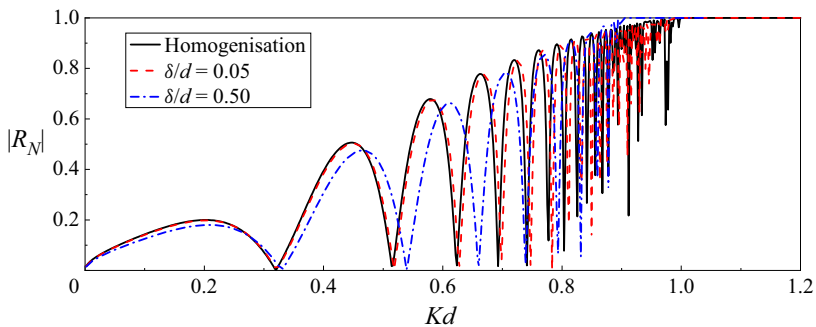

Figure 8. The variation of the modulus of reflection coefficient $|R_N|$ for the discrete model and the continuum model against the non-dimensional wavenumber Kd for the case of $N\delta = h$ and $d/h = 0.2$.
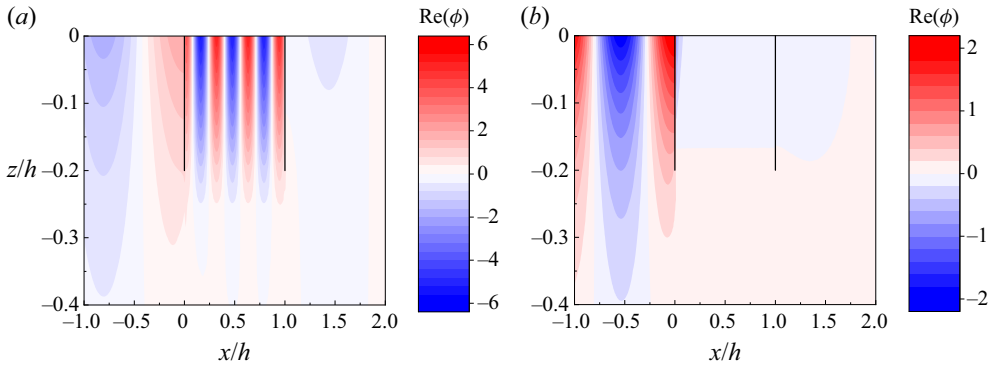
Figure 9. The fields of the real part of the velocity potential for the continuum model with $d/h = 0.2$ and $N\delta = h$: (a) $Kd = 0.8$; (b) $Kd = 1.2$.

which occur as the critical frequency is approached, mean that the models diverge for Kd sufficiently close to one. The continuum model serves as a good approximation for the spacing $\delta/d < 0.05$ when $Kd \lesssim 0.7$ or $\delta/d < 0.5$ when $Kd \lesssim 0.4$.

Finally, in figure 9 we plot the velocity potential field for two cases of scattering of incident waves by a barrier array computed using the continuum model for $d/h = 0.2$ and $N\delta = h$ at $Kd = 0.8$ and $Kd = 1.2$, that is, above and below the critical frequency respectively. In the first case, we can see wave propagation through the barrier array leading to transmission beyond the array. In the second case, we see rapid decay of the wave field through the array and near perfect reflection of incident waves. We have been unable to show a field plot from the direct numerical approach since the solution to the scattering problem requires that we used the second method presented in § 2 to determine eigenfunctions. As explained at the end of § 2.3, this method is poor at producing convergent representations for the field.

6. Conclusions

The main focus of this paper has been on describing and comparing two approaches to solving the problem of two-dimensional wave propagation through periodic arrays of surface-piercing barriers with a particular focus on the small spacing between adjacent barriers. A continuum model is described which is derived formally for small barrier spacing using homogenisation methods. This model is shown to be valid away from resonance occurring at $\omega = \sqrt{g/d}$; the propagating wavelength is predicted to become vanishingly small as resonance is approached, signalling a breakdown in the multiple-scale assumption underpinning homogenisation. This conclusion sheds light on previously unexplained ill-posed behaviour associated with the use of a continuum description for wave interaction with resonance in plate arrays in problems encountered by, for example, Jan & Porter (2018) and Zheng *et al.* (2020). A more complicated approach is based on an exact description of the barrier array for non-zero spacing, δ. First, by considering propagation in infinite periodic barrier arrays we have been able to show that there is a critical frequency ω_c which lies below $\sqrt{g/d}$ and acts to divide wave propagation from wave decay. At the critical frequency, standing waves exist between the barriers in the array and carry no energy. As $\delta \to 0$, this model tends to the continuum model provided frequencies are sufficiently far away from resonance. The approach shows that, for a

960 A20-30

non-zero spacing, there is a well-behaved transition from passing to stopping associated with wavelengths on the scale of the separation δ.

The exact description in terms of non-zero δ for a finite number of $N + 1$ barriers is also considered. Use is made of an orthogonality relation which applies to eigenmodes derived from the infinite periodic array to express the solution through the entire finite barrier array region in terms of the solution in just one period. The results show that the limit of the discrete problem is the continuum problem provided resonance is avoided.

Although this problem has been developed for a simple geometry where extensive use of separation of variables has been made to develop a semi-analytical approach to the problem in terms of solutions to a pair of scalar integral equations, it is clear that there will be other problems in water waves, linearised acoustics, etc. involving scattering by finite periodic arrays which can be analysed by the same method. In particular, the orthogonality condition satisfied by the eigenfunctions for the periodic Bloch problem is key to connecting solutions from one edge of a periodic array to the other. Its construction is in § 2.1 of the paper, which is not dependent on the geometry of the structure and can be applied to fields governed by the Helmholtz equation, for example.

Following this work, it would be interesting to consider wave propagation through an array of barriers in which the barrier length is a slowly varying function of space. For example, the methods described by Porter (2020) could be used to transform the scattering process into an ordinary differential equation in the continuum limit $\delta \to 0$ as a means of qualitatively understanding the onset of resonance/rainbow reflection in graded arrays such as those described by Wilks *et al.* (2022).

Declaration of interests. The authors report no conflict of interest.

Author ORCIDs.
J. Huang https://orcid.org/0000-0002-5387-3193;
R. Porter https://orcid.org/0000-0003-2669-0188.

Appendix A. Numerical treatment for the slowly convergent series in L_{mn} and K_{mn}

In § 2.3, the matrices formed by L_{mn} and K_{mn} are presented for determining the Bloch–Floquet wavenumber β. It can be found that all of the series in L_{mn} and K_{mn} are convergent as of $O(1/r^2)$. In order to speed up the series convergence, the last term in (2.40) (taken as an example) can be written as

$$
\sum_{r=-\infty}^{\infty} l_{mn,r} = l_{mn,0} + \frac{[1 + (-1)^{m+n}]^2}{24\pi}
$$
$$
+ \sum_{r=1}^{\infty} \left[l_{mn,r} - \frac{\cos\left[\frac{1}{2}(m-n)\pi\right] + \sin\left[\beta\delta - \frac{1}{2}(m+n)\pi\right]}{2r^2\pi^3} \right]
$$
$$
+ \sum_{r=-\infty}^{-1} \left[l_{mn,r} - (-1)^{m+n} \frac{\cos\left[\frac{1}{2}(m-n)\pi\right] - \sin\left[\beta\delta + \frac{1}{2}(m+n)\pi\right]}{2r^2\pi^3} \right],
$$
(A1)

with

$$l_{mn,r} = \frac{J_m\left(\frac{1}{2}\beta_r\delta\right) J_n\left(\frac{1}{2}\beta_r\delta\right)}{\beta_r\delta \tanh \beta_r(h-d)},$$ (A2)

where the asymptotic form of Bessel function has been used, i.e. $J_n(z) \sim \sqrt{2/(\pi z)}$ $\cos(z - n\pi/2 - \pi/4)$ when $|z| \to \infty$ and $|\arg z| < \pi$ (see Abramowitz & Stegun 1972). The infinite series in (A1) now decay like $O(1/r^4)$ such that results can be efficiently computed to high accuracy (we aim for an error of less than 10^{-8}). For other slowly convergent series, we apply the same treatment.

REFERENCES

ABRAMOWITZ, M. & STEGUN, I. 1972 *Handbook of Mathematical Functions*. US Department of Commerce.

AN, Z. & YE, Z. 2004 Band gaps and localization of water waves over one-dimensional topographical bottoms. *Appl. Phys. Lett.* **84** (15), 2952–2954.

ARCHER, A.J., WOLGAMOT, H.A., ORSZAGHOVA, J., BENNETTS, L.G., PETER, M.A. & CRASTER, R.V. 2020 Experimental realization of broadband control of water-wave-energy amplification in chirped arrays. *Phys. Rev. Fluids* **5** (6), 62801.

BENNETTS, L.G., PETER, M.A. & CRASTER, R.V. 2018 Graded resonator arrays for spatial frequency separation and amplification of water waves. *J. Fluid Mech.* **854**, R4.

CHEN, L., KUO, C., YE, Z. & SUN, X. 2004 Band gaps in the propagation and scattering of surface water waves over cylindrical steps. *Phys. Rev.* E **69** (6), 066308.

COLQUITT, D.J., COLOMBI, A., CRASTER, R.V., ROUX, P. & GUENNEAU, S. 2017 Seismic metasurfaces: sub-wavelength resonators and Rayleigh wave interaction. *J. Mech. Phys. Solids* **99**, 379–393.

CRASTER, R.V., KAPLUNOV, J. & PICHUGIN, A.V. 2010 High-frequency homogenization for periodic media. *Proc. R. Soc.* A **466**, 2341–2362.

DUPONT, G., REMY, F., KIMMOUN, O., MOLIN, B., GUENNEAU, S. & ENOCH, S. 2017 Type of dike using c-shaped vertical cylinders. *Phys. Rev.* B **96**, 180302.

ERDÉLYI, A., MAGNUS, W., OBERHETTINGER, F. & TRICOMI, F.G. 1954 *Tables of Integral Transforms*. McGraw-Hill.

EVANS, D.V. 1978 The oscillating water column wave-energy device. *J. Inst. Maths Applics.* **22**, 423–433.

EVANS, D.V. & MORRIS, C.A.N. 1972 Complementary approximations to the solution of a problem in water waves. *IMA J. Appl. Maths* **10** (1), 1–9.

EVANS, D.V. & PORTER, R. 1997 Complementary methods for scattering by thin barriers. In *Mathematical Techniques for Water Waves*. Computational Mechanics.

GARNAUD, X. & MEI, C.C. 2009 Wave-power extraction by a compact array of buoys. *J. Fluid Mech.* **635**, 389–413.

JAN, A.U. & PORTER, R. 2018 Transmission and absorption in a waveguide with a metamaterial cavity. *J. Acoust. Soc. Am.* **144** (6), 3172–3180.

JIMÉNEZ, N., ROMERO-GARCIA, V., PAGNEUX, V. & GROBY, J.P. 2017 Rainbow-trapping absorbers: broadband, perfect and asymmetric sound absorption by subwavelength panels for transmission problems. *Sci. Rep.* **7**, 13595.

KO, D.Y.K. & SAMBLES, J.R. 1988 Scattering matrix method for propagation of radiation in stratified media: attenuated total reflection studies of liquid crystals. *J. Opt. Soc. Am.* A **5** (11), 1863–1866.

LINTON, C.M. 2011 Water waves over arrays of horizontal cylinders: band gaps and Bragg resonance. *J. Fluid Mech.* **670**, 504–526.

LINTON, C.M. & MCIVER, P. 2001 *Handbook of Mathematical Techniques for Wave/Structure Interactions*. Chapman & Hall CRC.

LIU, T., LIANG, S., CHEN, F. & ZHUA, J. 2018 Inherent losses induced absorptive acoustic rainbow trapping with a gradient metasurface. *J. Appl. Phys.* **123**, 091702.

MA, G. & SHENG, P. 2016 Acoustic metamaterials: from local resonances to broad horizons. *Sci. Adv.* **2** (2), e1501595.

MCIVER, P. 1985 Scattering of water waves by two surface-piercing vertical barriers. *IMA J. Appl. Maths* **35** (3), 339–355.

MCIVER, P. 2000 Water-wave propagation through an infinite array of cylindrical structures. *J. Fluid Mech.* **424**, 101–125.

MEI, C.C., STIASSNIE, M.A. & YUE, D.K. 2005 *Theory and Applications of Ocean Surface Waves: Part 1: Linear Aspects*. World Scientific.

NEWMAN, J.N. 1974 Interaction of water waves with two closely spaced vertical obstacles. *J. Fluid Mech.* **66**, 97–106.

PORTER, R. 2020 On the connection between step approximations and depth-averaged models for wave scattering by variable bathymetry. *Q. J. Mech. Appl. Maths* **73** (1), 84–100.

PORTER, R. 2021 Modelling and design of a perfectly-absorbing wave energy converter. *Appl. Ocean Res.* **113**, 102724.

PORTER, R. & EVANS, D.V. 1995 Complementary approximations to wave scattering by vertical barriers. *J. Fluid Mech.* **294**, 155–180.

PORTER, R. & PORTER, D. 2003 Scattered and free waves over periodic beds. *J. Fluid Mech.* **483**, 129–163.

PORTER, R., ZHENG, S. & LIANG, H. 2022 Scattering of surface waves by vertical truncated structured cylinders. *Proc. R. Soc.* A **478**, 20210824.

ROY, R., DE, S. & MANDAL, B.N. 2019 Water wave scattering by multiple thin vertical barriers. *J. Acoust. Soc. Am.* **355**, 458–481.

TANG, S.K. 2012 Narrow sidebranch arrays for low frequency duct noise control. *J. Acoust. Soc. Am.* **132** (2), 3086–3100.

URSELL, F. 1947 The effect of a fixed vertical barrier on surface waves in deep water. *Math. Proc. Camb. Phil. Soc.* **43** (3), 374–382.

WILKS, B., MONTIEL, F. & WAKES, S. 2022 Rainbow reflection and broadband energy absorption of water waves by graded arrays of vertical barriers. *J. Fluid Mech.* **941**, A26.

YANG, S., WU, F., ZHONG, H. & ZHONG, L. 2006 Large band gaps of water waves through two-dimensional periodic topography. *Phys. Lett.* A **352** (4–5), 426–430.

ZHENG, S., PORTER, R. & GREAVES, D. 2020 Wave scattering by an array of metamaterial cylinders. *J. Fluid Mech.* **903**, A50.